U.PORTO
FACULDADE DE CIÊNCIAS
UNIVERSIDADE DO PORTO

U.PORTO
ICBAS | INSTITUTO DE CIÊNCIAS BIOMÉDICAS ABEL SALAZAR
SCHOOL OF MEDICINE AND
BIOMEDICAL SCIENCES

U.PORTO
FACULDADE DE CIÊNCIAS
UNIVERSIDADE DO PORTO

U.PORTO
ICBAS | INSTITUTO DE CIÊNCIAS BIOMÉDICAS ABEL SALAZAR
SCHOOL OF MEDICINE AND
BIOMEDICAL SCIENCES

In vivo and *in vitro* characterization of a bacterial transporter

Inês Rosa Figueiredo da Costa

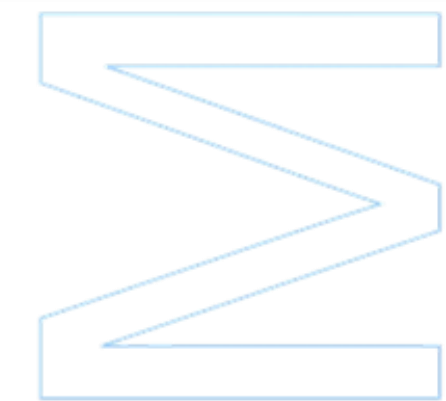Dissertação de Mestrado apresentada à

Faculdade de Ciências da Universidade do Porto e Instituto de

Ciências Biomédicas Abel Salazar

Bioquímica

2022

In vivo and *in vitro* characterization of a bacterial transporter

Inês Rosa Figueiredo da Costa

Mestrado em Bioquímica
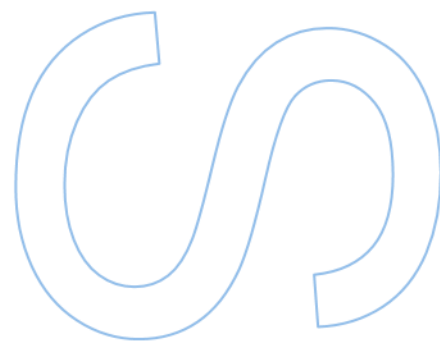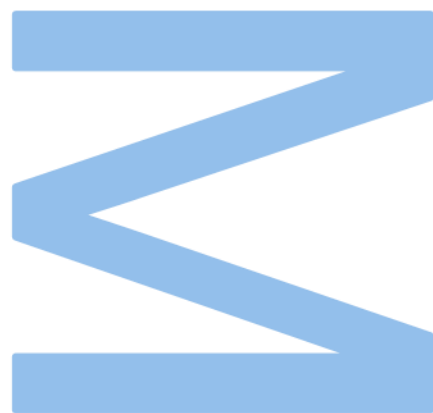Faculdade de Ciências da Universidade do Porto e Instituto de Ciências Biomédicas Abel Salazar
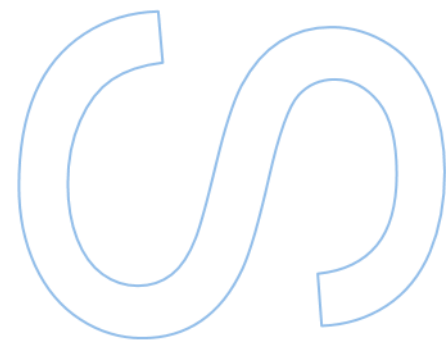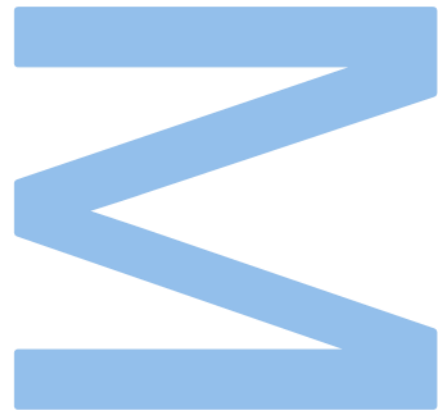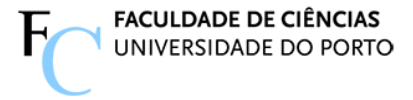2022

Orientador
João Morais Cabral, Investigador Principal, i3s

Coorientadora
Marta Vaz Mendes, Professora Auxiliar Convidada, ICBAS

Declaração de Honra

Eu, Inês Rosa Figueiredo da Costa, inscrito(a) no Mestrado em Bioquímica da Faculdade de Ciências da Universidade do Porto declaro, nos termos do disposto na alínea a) do artigo 14.º do Código Ético de Conduta Académica da U.Porto, que o conteúdo da presente dissertação de projeto reflete as perspetivas, o trabalho de investigação e as minhas interpretações no momento da sua entrega.

Ao entregar esta dissertação de projeto, declaro, ainda, que a mesma é resultado do meu próprio trabalho de investigação e contém contributos que não foram utilizados previamente noutros trabalhos apresentados a esta ou outra instituição.

Mais declaro que todas as referências a outros autores respeitam escrupulosamente as regras da atribuição, encontrando-se devidamente citadas no corpo do texto e identificadas na secção de referências bibliográficas. Não são divulgados na presente dissertação de projeto quaisquer conteúdos cuja reprodução esteja vedada por direitos de autor.

Tenho consciência de que a prática de plágio e auto-plágio constitui um ilícito académico.

Inês Rosa Figueiredo da Costa

Porto, 7 de Dezembro de 2022

Agradecimentos

Antes de mais, gostaria de expressar a minha gratidão a todas as pessoas sem as quais a concretização desta dissertação não seria possível:

Ao meu orientador, Dr. Morais Cabral, por me ter dado a oportunidade de ter participado neste projecto, por ter acreditado em mim e a pela compreensão que teve pelas minhas limitações. Agradeço todo o conhecimento que me transmitiu e pelas competências que me incentivou a desenvolver.

À Dra. Carol Harley, por toda a ajuda prestada, pela paciência, pelo esclarecimento de dúvidas, pela sabedoria que me transmitiu.

À Andreia Fernandes e à Katharina Weishäupl por estarem sempre dispostas a ajudar. À Tatiana Cereija, um agradecimento especial por todo o tempo que disponibilizou para estar comigo a ajudar-me, pelas ideias e sugestões partilhadas, pela companhia. À Marta Costa desejo a continuação de um percurso académico gratificante. A todas agradeço pelo ambiente de amizade e interajuda que este grupo cultiva.

Ao meu irmão Afonso, pelo qual nutro o maior orgulho, que me inspira a ser uma pessoa melhor e que me relembra da importância de mantermos o nosso conhecimento actualizado, tanto a nível científico como a nível geral.

Ao Zé, pelo companheirismo e apoio incondicional, agradeço por tudo.

Resumo

O potássio é o elemento predominante no meio intracelular da bactéria, intervindo em vários processos homeostáticos, tais como osmorregulação, regulação do pH e função enzimática. De forma a cumprir estas funções, os iões de potássio (K^+) são transportados através da membrana, tanto de forma passiva através de canais, bem como de forma activa por transportadores. YjbQ é um transportador de K^+ que pode ser encontrado em *Bacillus subtilis*, uma das bactérias Gram-positivas mais estudadas. O YjbQ é classificado como antiportador K^+/H^+, de acordo com a base de dados Subtiwiki devido à sua semelhança com o SaCpaA de *Staphylococcus aureus*. YjbQ contém um regulador de condutância de K^+ (RCK) no seu C-terminal. Os domínios RCK podem regular canais e transportadores de K^+ em resposta a iões e nucleótidos, tais como o c-di-AMP. Mais especificamente, c-di-AMP é um mensageiro secundário envolvido em metabolismo, formação de biofilmes e integridade do DNA. O c-di-AMP tem sido proposto como activador da actividade do YjbQ, à semelhança de outro K^+/H^+ antiportador em *B. subtilis*, o KhtTU. Estudos anteriores no nosso laboratório confirmaram que o c-di-AMP se liga ao sub-domínio RCK_C do YjbQ. O principal objectivo deste trabalho foi caracterizar os aspectos funcionais do YjbQ, em particular perceber de que maneira a actividade deste transportador é afectada pelas variações de pH, compreender se a presença do YjbQ é vantajosa em situações de stress alcalino e/ou ácido, identificar quais os iões que são selectivamente transportados, e determinar o efeito da ligação do c-di-AMP na actividade de transporte. Desta feita, foram realizados ensaios de fluxo baseados em monitorização de fluorescência a partir de vesículas evertidas, bem como testes de crescimento em *B. subtilis*. Os resultados indicam que o YjbQ apresenta uma preferência pelo transporte de iões de potássio, mas permitindo também a passagem de iões de sódio, e apresenta um melhor desempenho a níveis de pH mais elevados. Além disso, ao contrário do que se esperava, os ensaios de fluxo demonstraram que o c-di-AMP inibe o transporte de K^+. Também testámos ortólogos do YjbQ de forma a explorar se se poderiam observar efeitos semelhantes, contudo sem sucesso. Os crescimentos em *B. subtilis* para testar a adaptabilidade a ambientes alcalinos e ácidos foram inconclusivos.

Palavras-chave: Iões de potássio (K^+), transporte de K^+, canal, transportador, antiportador, domínio RCK, c-di-AMP, YjbQ, *Bacillus subtilis*

Abstract

Potassium, the most prevalent element in the bacterial intracellular environment, is involved in numerous homeostatic processes, namely osmoregulation, regulation of pH and enzymatic function. To fulfil these roles, potassium ions (K^+) are transported across the membrane, either passively through channels or actively through transporters. YjbQ is a K^+ transporter found in *Bacillus subtilis,* one of the best characterized Gram-positive bacteria, currently classified as a K^+/H^+ antiporter in the Subtiwiki database due to its similarity to SaCpaA from *Staphylococcus aureus*. YjbQ contains a regulator of conductance of $\underline{K^+}$ (RCK) in its C-terminus. RCK domains can regulate K^+ channels and transporters in response to ions and nucleotides, such as c-di-AMP, which is a second messenger involved in metabolism, biofilm formation and DNA integrity. It is proposed that c-di-AMP activates transport in YjbQ, mirroring the other *B. subtilis* K^+/H^+ antiporter KhtTU. Previous research in our laboratory confirmed that c-di-AMP binds to the RCK_C sub-domain of YjbQ. The main goal of this work was to characterize the functional aspects of YjbQ, to assess how the activity of this transporter is affected by variations in pH and whether the presence of YjbQ is advantageous in situations of alkaline and acidic stress, to identify which ions are selectively transported, and to determine the effect of c-di-AMP binding on transport activity. For this purpose, fluorescent-based flux assays from everted vesicles were performed, as well as growth tests in *B. subtilis*. The results indicate that YjbQ exhibits a preference for the transport of potassium ions, while also allowing the passage of sodium ions, and performs better at higher pH levels. Moreover, contrary to what was expected, fluorescence-based flux assays demonstrated that c-di-AMP inhibits K^+ transportation, both from everted vesicles produced with wild-type protein and with a mutated version lacking a residue crucial to the binding event. Orthologs of YjbQ were also tested to explore whether similar effects could be observed, however without success. Growths in *B. subtilis* to test adaptability to alkaline and acidic environments were inconclusive.

Keywords: Potassium ions (K^+), K^+ transport, channel, transporter, antiporter, RCK domain, c-di-AMP, YjbQ, *Bacillus subtilis*

Table of contents

List of Tables

List of Figures

List of Abbreviations

ACMA	9-amino-6-Chloro-2-Methoxyacridine
ADP	Adenosine diphosphate
APC	Amino acid-polyamine-organocation superfamily
ATP	Adenosine triphosphate
BSA	Bovine Serum Albumin
cAMP	Cyclic adenosine monophosphate
cGAMP	Cyclic guanosine monophosphate–adenosine monophosphate
c-di-AMP	Cyclic di-adenosine monophosphate
c-di-GMP	Cyclic di-guanosine monophosphate
CPA	Cation/proton antiporter
CPA1	Cation/proton Antiporter 1 subfamily
CPA2	Cation/proton Antiporter 2 subfamily
DAC	Diadenylate cyclase
DNA	Deoxyribonucleic acid
DRaCALA	Differential Radial Capillary action of Ligand Assay
DTT	Dithiothreitol
HEPES	4-(2-hydroxyethyl)-1-piperazineethanesulfonic acid
LB	Lysogeny Broth
LB-BS	Lysogeny Broth adapted for *Bacillus subtilis*
LBK	Lysogeny broth with K^+
LBK-BS	Lysogeny Broth with K^+ adapted for *Bacillus subtilis*
OD	Optical density
pApA	Phosphoadenylyl Adenosine
PCR	Polymerase Chain Reaction
PDB	Protein Data Bank
PDE	Phosphodiesterases
(p)ppGpp	Guanosine pentaphosphate and tetraphosphate
RCK	Regulator of conductance of K^+
RCK_C	RCK domain C-terminal subdomain
RCK_N	RCK domain N-terminal subdomain
RNA	Ribonucleic acid
rpm	Revolutions per minute
SMM	Spizzen Minimal Medium

TAE	Tris-Acetate-EDTA
Tris	Tris(hydroxymethyl)aminomethane
YPD	Yeast extract, Peptone, Dextrose

1.Introduction

1.1 Potassium

1.1.1 Physiological roles

Potassium ions (K^+) are the most prevalent monovalent cations in the cytosol, being accumulated in all cells (Beagle & Lockless, 2021) across the kingdoms of life (Diskowski et al., 2017).

Potassium ions are essential for the survival of bacteria, with various roles in osmoregulation, balancing pH levels, electrical signaling, membrane potential regulation, enzyme activity and protein synthesis (Stautz et al., 2021). In particular, K^+ is necessary for ensuring ribosomal structural (Beagle & Lockless, 2021) and functional integrity (Gundlach et al., 2017), which is essential for protein synthesis to occur (Beagle & Lockless, 2021). This cation is also implicated in regulation of pH levels as it is exchanged with H^+ and acts as a counterion to glutamate and to the negative charge of nucleic acids (Gundlach et al., 2017).

Additionally, turgor pressure, meaning the pressure that intracellular water exerts on the cell wall, is managed by osmoregulatory processes (Zarrella & Bai, 2020) which involve K^+. In particular, K^+ is accumulated in response to hyperosmotic stress (Beagle & Lockless, 2021) as an initial fast osmoprotective response (Stülke & Krüger, 2020). However, higher than ideal intracellular levels of this cation may have negative consequences, particularly in protein synthesis and function (Holtmann et al., 2003). To solve this issue for long-term adaption (Stülke & Krüger, 2020), during the second phase of osmoadaptation (Holtmann et al., 2003) bacteria extrude potassium ions while accumulating compatible solutes, which are molecules that do not affect cellular functioning even at large concentrations and that may be obtained from the environment or synthesized by bacteria (proline, glycine betaine, carnitine, proline betaine, or trehalose) (Stülke & Krüger, 2020). In a nutshell, K^+ enters the cells together with the production or uptake of suitable solutes to prevent dehydration as the external osmolarity rises. When the osmolarity of the environment drops, K^+ and other compatible solutes are released to stop cell lysis (Zarrella & Bai, 2020).

Potassium ions also influence the development of biofilms (Prindle et al., 2015), with lower concentrations of the cation inducing its formation (Zarrella & Bai, 2020). Biofilms are coordinate structures made of bacterial aggregates immersed in matrixes of extra-cellular substances, such as adhesins or polysaccharides (Earl et al., 2008; Prindle et al., 2015; Zarrella & Bai, 2020), that provide survival advantages, by offering protection

against antimicrobials and by promoting adherence to animal or plant tissues (Zarrella & Bai, 2020).

1.1.2 K⁺ transport

In order to accomplish all of these functions and considering that potassium ions become toxic at higher concentration levels, bacteria need to control the K^+ intracellular levels (Beagle & Lockless, 2021). This is achieved through transport proteins that act as systems of import and export of potassium (Stautz et al., 2021). Ions are unable to freely diffuse across the membrane due to their charges (Beagle & Lockless, 2021), so transport occurs either passively through ion channels, simply allowing ions to flow down the electrochemical gradient, or actively through transporters, requiring ATP or the electrochemical gradient of a co-transported molecule or ion, including the H^+ gradient formed as part of the proton motive force (Stautz et al., 2021). The proton motive force (PMF) is the energy generated by the transfer of H^+ across the bacterial cell membrane (Krulwich et al., 2011). It can be arithmetically expressed as the result of adding the transmembrane electrical potential difference and a pH difference (Bakker & Mangerich, 1981). The PMF produced by proton pumps can be used by active transporters to provide the necessary energy for transport to occur (Krulwich et al., 2011).

Although the definition of a channel or a transporter is quite clear, it is not always straightforward to distinguish their molecular mechanisms; nonetheless, it is still possible to define some distinctions between them. Ion channels tend to have pores through which ions pass when a gate is opened and the electrochemical gradient is favorable. Transporters tend to go through conformational changes that involve the alternated opening of two gates to allow the passage of the ions (Figure 1). These conformational changes are associated with energy provided by other co-occurring phenomenon, such as binding of a co-transported molecule or ATP hydrolysis. Importantly, this energy input allows transporters to promote the movement of ions against their electrochemical gradient, unlike ion channels (Ashcroft et al., 2009). However, sometimes a membrane protein can be initially considered an active transporter, only later to be found out that it was an ionic channel, as it happened in the case of the KtrAB cation channel for instance (Stautz et al., 2021).
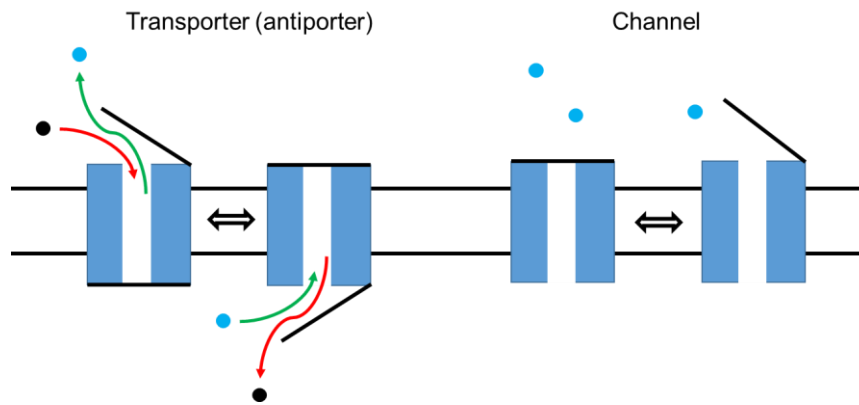
Figure 1: Representation of some differences between transporters and channels. Transporters have two gates that open in a coordinated and alternated fashion and channels only one. Blue and black spheres represent ionic species.

There are many K$^+$ channels and transporters. A few examples are discussed below.

1.1.2.1   K$^+$ channels

K$^+$ channels allow the passage of potassium across the membrane down their electrochemical gradient (Cuello et al., 1998). These channels have a pore-forming domain associated with transport, and a sensory regulatory domain. K$^+$ channels are tetramers, and each of the respective subunits contains two transmembrane helices that contribute to the formation of the ionic pathway (Figure 2) (Kuang et al., 2015). Ion channels are highly selective for K$^+$ over Na$^+$ (Shrivastava et al., 2002), due to the properties of the narrowest part of the pore, the selectivity filter (MacKinnon, 2003). However, Na$^+$ may be able to pass as well if the chance is given. This ion preference stems from differences in their size, associated to ionic radii, and from their coordination with chemical groups in the selectivity filter (Shrivastava et al., 2002).

The flux of ions across channels is regulated through gating, usually by cytoplasmic domains sensitive to cellular signals (Roosild et al., 2009). Some K$^+$ channels are ligand-gated, with the pore opening or closing due to the binding of an ion or a molecule. Others are voltage-gated, with the pore opening or closing in response to the membrane electric field (MacKinnon, 2003), while others are pH-gated, with the protonation of residues of the channel being the cause of the pore opening event (Cuello et al., 1998). Regarding the closure of the pores, there are also two other gating models, slow inactivation through the C-type mechanism and fast inactivation through the N-type mechanism (or Ball and Chain model). In the N-type inactivation, a cytoplasmic region binds to a site nearby the

open pore, blocking the passage of the ions (Goldin, 2003). In the C-type mechanism, the inactivation comes from the selectivity filter itself (Cuello et al., 2010).

In terms of K$^+$ uptake in bacteria, the KtrAB and TrkAH proteins are found in most bacteria, intervening in pH, membrane potential and osmotic regulation (Stautz et al., 2021). TrkAH is a complex (Epstein, 2003), composed by the TrkH membrane protein, responsible for K$^+$ uptake, and its regulatory protein, TrkA, which closes the channel when bound to ADP and opens it when bound to ATP (Zhang et al., 2020). TrkAH was initially described as an active transporter and later was shown to be an ATP- and ADP-gated ion channel instead. The same case happened with KtrAB, which was initially thought to be a symporter or antiporter, only later to be revealed that actually functions as a channel (Stautz et al., 2021). KtrAB includes two subunits, the membrane-associated KtrA, related to TrkA, and the membrane-embedded KtrB related to TrkH (Holtmann et al., 2003; Corrigan & Gründling, 2013). KtrA is a member of the RCK family (see below, Section 1.1.3: Figure 4) and is composed by an N-terminal RCK_N domain, where ATP binding occurs, and a C-terminal RCK_C domain, where c-di-AMP binding occurs (Corrigan & Gründling, 2013), being the first identified c-di-AMP binding protein (Fahmi et al., 2017). The uptake of K$^+$ performed by KtrAB is particularly important during higher osmotic stress in *B. subtilis* (Holtmann et al., 2003).
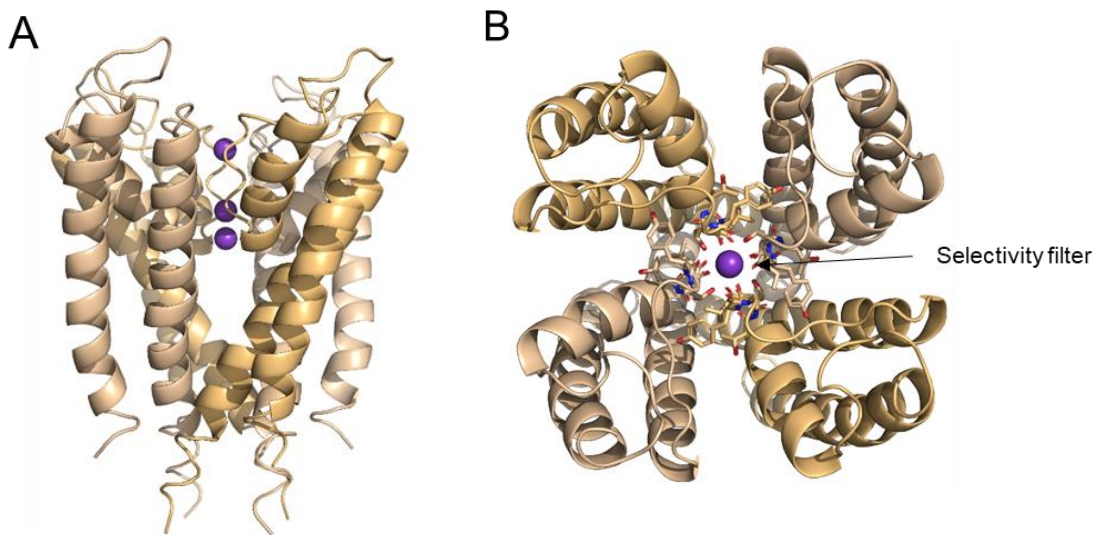
Figure 2: Two views of the structure of a potassium channel (KcsA from *Streptomyces lividans* of Doyle et al. (1998)). A: Lateral view from the membrane. B: Top view from the periplasm. The channel representation shows 4 identical subunits with alternate colors to facilitate visualization. The purple spheres represent potassium ions. The selectivity filter located in the external half of the pore, is the narrowest part of the pore and is indicated with an arrow. This image was created with PyMOL using a PDB code (1BL8).

1.1.2.2   K⁺ transporters

Intracellular K⁺ can also be regulated by import and export performed by ion transporters (Roosild et al., 2009). There are primary and secondary transporters. Primary active transporters associate the movement of ions to an energy source, such as ATP hydrolysis (Boudker & Verdon, 2010), and KdpFABC is an example of this kind (Stautz et al., 2021). On the other hand, secondary active transporters associate the electrochemical gradient of one ionic species to the movement of another one (Forrest et al., 2021). Kup, KimA and KhtTU, for instance, are secondary active K⁺ transporters that promote the co-movement of K⁺ and H⁺ (Stautz et al., 2021).

The primary active transporter KdpFABC (Figure 3), characterized in *Escherichia coli*, is a K⁺ pump driven by ATP hydrolysis (Stautz et al., 2021) consisting of four membrane proteins with high affinity and specificity for K⁺. KdpF is important for stability, though not for function (Epstein, 2003). KdpA and KdpB are the subunits that allow the passage of K⁺ across the membrane (Stock et al., 2018). In addition, the P-type ATPase KdpB is responsible for the ATP hydrolysis driving K⁺ translocation (Stautz et al., 2021), and contains a regulatory phosphorylation site. KdpC seems to intervene in the assembly of the complex (Epstein, 2003) and in the binding of substrates. KdpFABC is regulated at a transcriptional level, and by phosphorylation when K⁺ concentrations stabilize (Stautz et al., 2021), since expression of this complex occurs mostly when other transport systems are unable to suitably uptake K⁺ (Epstein, 2003).
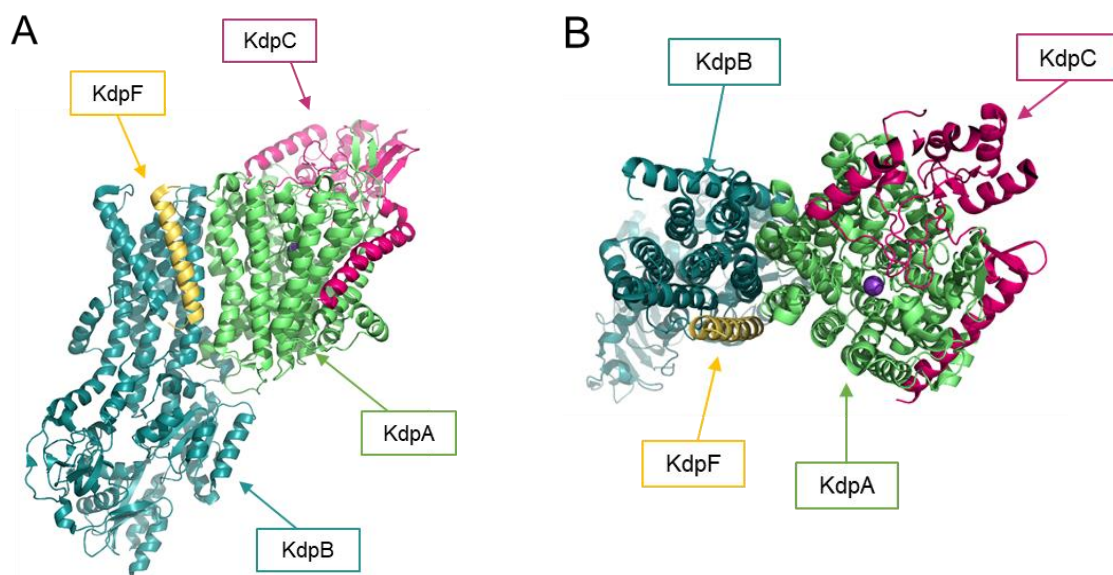
Figure 3: Two views of the structure of KdpFABC of Stock et al. (2018). A: Lateral view from the membrane. B: Top view from the periplasm. Each subunit is shown in a different color: KdpA in green, KdpB in blue, KdpC in pink and KdpF in yellow. The purple sphere represents a K⁺. Image was created with PyMOL using a PDB code (5MRW).

Secondary active transporters KimA and Kup belong to the KUP family of bacterial transporters, which in turn belongs the APC superfamily. KimA and Kup are K^+/H^+ symporters, which means these transporters move K^+ against its concentration gradient, through proton transport down its electrochemical gradient in the same direction (Stautz et al., 2021). KimA has high-affinity for potassium (Tascón et al., 2020) and the activity of Kup and KimA is more robust at lower pH levels, and inhibited by high osmolarity conditions (Epstein, 2003).

Cation/proton antiporters (CPAs) lead to the exchange of cations for one or more protons. They are found in many species including humans and play important roles in maintaining pH homeostasis and osmoregulation. CPAs are divided into CPA1 and CPA2 due to whether they are electroneutral (CPA1) or electrogenic (CPA2) (Masrati et al., 2018). One example of CPA is K^+/H^+ antiporter KhtTU. KhtU is a membrane protein from the CPA2 superfamily, and KhtT is a cytoplasmic protein. c-di-AMP binds at the RCK_C domain of KhtT, activating transport of K^+. The activity of this complex increases at higher pH levels, achieving a maximum at pH 9.0, thereby promoting the adaptation of bacteria to alkaline environments. KhtTU is selective towards potassium, when compared to sodium transportation (Cereija et al., 2021), yet it still allows the transport of rubidium (Fujisawa et al., 2007).

1.1.3 RCK domains

Potassium channels and transporters may contain regulators of conduction of K^+ (RCK) domains that, as the name suggests, correspond to the cytosolic domains that regulate K^+ flow (Giraldez & Rothberg, 2017). RCK domains are found in more than half of all prokaryotic K^+ channels and in many transporters (Teixeira-Duarte et al., 2019), and they have also been discovered in eukaryotic K^+ channels (Giraldez & Rothberg, 2017). RCK domains combine as functional octameric rings out of dimeric or pseudo-dimeric units and are classified as cation- or nucleotide-dependent, according to the binding substrate (Teixeira-Duarte et al., 2019). The subunit structure (Figure 4) displays a Rossman fold at the RCK_N domain, characterized as alternation between alpha helices and beta strands, with the final helix intercalated as a crossover helix into the RCK_N domain of the other subunit in the dimer. The RCK_C domain follows the crossover helix and interacts with the RCK_C domain of the other dimer subunit (Albright et al., 2006). When the ligand binds to the RCK domains of channels, a conformational change in the octamer is induced due to the rearrangement within the dimers that leads to increase flexibility of linkers, transmitting a mechanical signal that allows the opening

of the pore through which potassium ions are able to flow (Diskowski et al., 2017; Albright et al., 2006). The RCK_C domain is found in various c-di-AMP-binding potassium transporters (Stülke & Krüger, 2020), where it functions as the binding site for c-di-AMP (Gundlach et al., 2019).
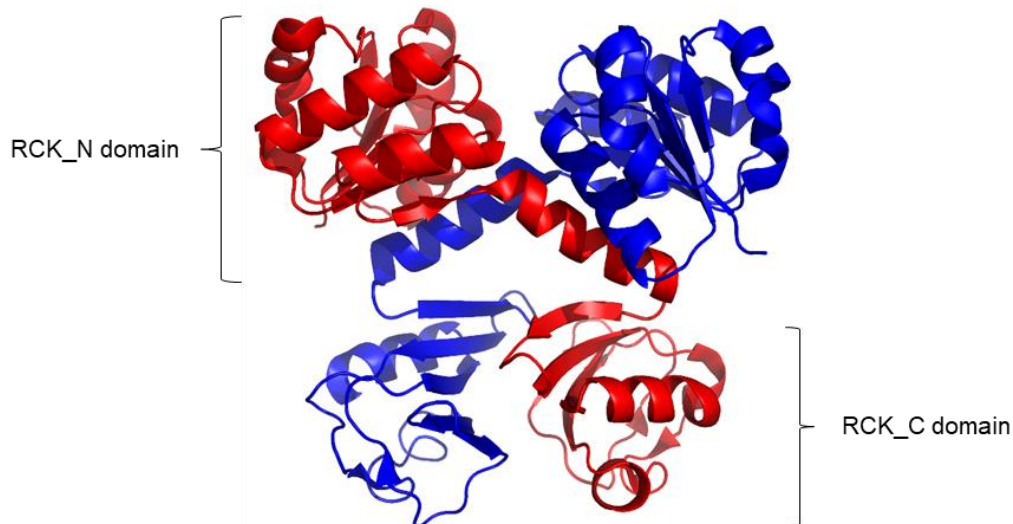
Figure 4: Representation of the structure of the RCK domain homodimer from potassium channel KtrAB. Individual subunits are shown in red and blue. The N and C subdomains of one of the monomers are indicated. This image was created with PyMOL using a PDB code (4J90), Vieira-Pires & Morais-Cabral (2013).

1.2   Cyclic-di-AMP (c-di-AMP)

Bacterial signaling, necessary for ensuring homeostasis, is carried out by two-component systems, sigma factors, riboswitches, transcription repressors and activators, posttranslational modifications (Stülke & Krüger, 2020), and second messengers. These molecules bind to cellular targets, changing their function and inducing a cellular response. Second messengers are usually present at low concentrations and its production, kept in balance by metabolic synthesis and degradation, increases when cells are stimulated (Kalia et al., 2013; Newton et al., 2016). In bacteria many of these molecules are mono- or dinucleotides (Stülke & Krüger, 2020). Nucleotides have crucial functions in cellular functioning, as building blocks to DNA and RNA and as energy sources, but also as important components of signaling pathways. These secondary messengers may be linear, such as guanosine tetra- or pentaphosphate (p)ppGpp produced under nutrient limitations, or cyclic (Corrigan & Gründling, 2013). Cyclic nucleotides include the well-known cyclic-AMP (cAMP), involved in carbon source utilization. Cyclic dinucleotides include cyclic di-GMP (c-di-

GMP), cyclic di-AMP (c-di-AMP), and cyclic GMP-AMP (cGAMP) (Stülke & Krüger, 2020).

c-di-AMP, two adenosine moieties bound through 3′,5′-phosphodiester linkages (Nelson et al., 2013), is found in many Gram-positive and some Gram-negative species (Zarrella & Bai, 2020). c-di-AMP is crucial for the survival of bacteria since this molecule has been linked to many functions of bacterial physiology (Zarrella & Bai, 2020), including genetic competence, antibiotic resistance, DNA repair (Stülke & Krüger, 2020) and maintenance of DNA integrity, biofilm formation, sporulation, metabolism, cell wall stress and osmotic homeostasis (Kalia et al., 2013; Nelson et al., 2013; Cereija et al., 2021). Disruption of c-di-AMP homeostasis results in a compromised cell growth. For example, individuals with mutations in the enzymes that produce c-di-AMP exhibited less resistance to DNA damaging agents such as methyl methane sulfate and to hydrogen peroxide induced oxidative stress (Zarrella & Bai, 2020). The formation of biofilms is also regulated by c-di-AMP (Stülke & Krüger, 2020).

The activity of diadenylate cyclases, phosphodiesterases, and exporters, which produce, degrade, and export c-di-AMP determine the levels of this molecule in cells (Stülke & Krüger, 2020). Diadenylate cyclases convert two molecules of ATP into c-di-AMP (Zarrella & Bai, 2020), with two molecules of pyrophosphate also being released (Stülke & Krüger, 2020). The only known protein domain that can catalyze the synthesis of c-di-AMP, and that all diadenylate cyclases possess, is the DAC domain (Stülke & Krüger, 2020). Besides the DAC domain, diadenylate cyclases have domains for protein localization, c-di-AMP synthesis regulation (Zarrella & Bai, 2020), and interaction domains (Stülke & Krüger, 2020). DAC domains are widespread across bacteria and archaea, and more than one diadenylate cyclase may be encoded by bacteria (Zarrella & Bai, 2020), however some species still lack these enzymes, and *E. coli* is an example of that (Stülke & Krüger, 2020). There are five main classes of diadenylate cyclases: CdaA, DisA, CdaS, CdaM and CdaZ (Stülke & Krüger, 2020). Most bacteria have only one type of diadenylate cyclase, while other have more; *B. subtilis*, for instance, has three of them (Fahmi et al., 2017), namely DisA, which regulates the integrity of replicated DNA, CdaA, which influences cell wall stress, and CdaS, which is selectively expressed during spore germination. c-di-AMP is broken down by phosphodiesterases (PDE) into AMP or phosphoadenylyl adenosine (pApA) (Zarrella & Bai, 2020). The classes of phosphodiesterases that degrade c-di-AMP are GdpP and PgpH, both found in *B. subtilis*, and Pde2 (Fahmi et al., 2017). Activity of phosphodiesterases is important to degrade c-di-AMP and avoid excessive accumulation that are reflected in increased susceptibility to stress (Stülke & Krüger, 2020). It should be taken into consideration the

fact that each species contains different cyclases, phosphodiesterases and receptors, which means that not all c-di-AMP signaling functions may be conserved across species (Zarrella & Bai, 2020).

Many c-di-AMP targets are involved in potassium homeostasis, in particular potassium channels and transporters. Moreover, intracellular K^+ levels are correlated with intracellular levels of this signaling molecule (Zarrella & Bai, 2020), with c-di-AMP concentration growing as intracellular K^+ levels increase (Gundlach et al., 2017). At higher potassium concentrations and with glutamate as the nitrogen source, the levels of c-di-AMP are at their maximum (Stülke & Krüger, 2020) and low intracellular K^+ levels correlate with low intracellular c-di-AMP concentrations (Zarrella & Bai, 2020). It is thought that the intracellular concentration of c-di-AMP drops and rises, in an effort to adapt to high and low osmotic pressure, corresponding to the increase and drop in potassium concentrations (Stülke & Krüger, 2020). Overall, it has been proposed that c-di-AMP inhibits K^+ import, by directly interacting with and/or controlling the expression of, for instance, Ktr/Trk, KimA, Kup, and Kdp systems, while activating K^+ export by SaCpaA (cation/proton antiporter A from *S. aureus*) and KhtTU (a K^+/H^+ antiporter from *B. subtilis*) (Zarrella & Bai, 2020). More information regarding *B. subtilis* and its potassium transporters is provided in the next sections.

1.3   *Bacillus subtilis*

1.3.1 Research and industrial appeal of *Bacillus subtilis*

Bacillus subtilis is one of the best-characterized Gram-positive bacterial species (Gu et al., 2019); while traditionally considered a strict aerobe, this has been disputed since this species also displays anaerobiosis (Nakano & Zuber, 1998). In response to environmental challenges, *B. subtilis* is able to generate endospores that endure harsh circumstances, such as high temperature, nutrient limitations, UV and γ-radiation (Kovács, 2019). The organisms may be isolated from both terrestrial and aquatic environments, and are able to exist as motile individuals or exhibit biofilm formation (Earl et al., 2008). *B. subtilis* has been used as a model for cell differentiation (Gu et al., 2019), sporulation (Zeigler et al., 2008), cell division, protein secretion, surface motility, biofilm formation, attachment to plants or fungi, and synthesis of secondary metabolites. Due to its capacity for uptake of extracellular DNA, which enables genetic alteration (Kovács, 2019)*,* and the availability of its genome sequence, research projects on *B. subtilis* are numerous. Various industrial procedures and academic studies use *B. subtilis* strains derived from strain 168, an auxotroph that needs tryptophan (Zeigler et al., 2008). *B.*

subtilis is used in enzyme production, synthesis of compounds such as vitamins, and food fermentation (Kovács, 2019), revealing probiotic qualities. Furthermore, this species has an adaptable metabolism that allows easy growth on cheap media, and is used in agriculture to promote crop development. The biofilms that *B. subtilis* forms are also able to synthesize compounds such as antibiotics (Su et al, 2020). Overall, *B. subtilis* has many applications and the study of this species is of great interest for industrial applications and the scientific community.

1.3.2 Potassium transportation in *Bacillus subtilis*

The intracellular potassium concentration of *B. subtilis* is kept around the value of 300 mM (Prindle et al., 2015) while the potassium concentrations in its habitat vary from 100 µM to 10 mM, so uptake systems are required to obtain and accumulate potassium ions (Gundlach et al., 2017). *B. subtilis* can live in habitats with low water availability and high salinity, leading to high osmolarity stress (Zaprasis et al., 2013). During hyperosmotic stress brought from dry salty soils, the intracellular K^+ concentration increases from 300 mM to around 600 (Whatmore et al., 1990), resisting loss of water and low turgor pressure (Hoffmann & Bremer, 2016). The import of compatible solutes is an additional contribute, for example via the Opu family of transporters, with OpuE leading to the import of proline (Zaprasis et al., 2013). On the other hand, when water influx caused by accumulation of potassium is excessive, increasing rapidly the turgor pressure, the integrity of the membrane may be compromised, therefore rapid export is a necessity for survival (Hoffman & Bremer, 2016), leading to a decrease of potassium concentration back to the regular 300 mM. Additionally, the control of the number of protons, that directly impact the pH level at a given moment, played by K^+/H^+ antiporters is important under alkaline stress, particularly when taken into consideration that *B. subtilis* is a neutralophilic species (Krulwich et al., 2011).

B. subtilis K^+ transport systems include the channels KtrAB, KtrCD, YugO, the K^+/H^+ symporter KimA, and the K^+/H^+ antiporters KhtTU and YjbQ (Stautz et al., 2021). Some of these are known targets of c-di-AMP; for example, c-di-AMP binds to the *ktrAB* and the *kimA* riboswitches, controlling transcription of these genes (Gundlach et al., 2019). Binding of c-di-AMP to KtrA or KtrC has been proposed to inhibit the activity of KtrAB and KtrCD but this has yet to be demonstrated experimentally (Gundlach at al., 2019). In contrast, it has been demonstrated that c-di-AMP binds to the RCK_C domain of KhtT activating the K^+/H^+ antiporter KhtTU (Cereija et al., 2021). Importantly, c-di-AMP has been proposed to bind also to YjbQ, the main focus of the present work.

1.3.3   YjbQ

YjbQ (or CpaA) is a membrane protein found in *B. subtillis*, currently classified as a K+/H+ antiporter in the Subtiwiki database due to its similarity to SaCpaA, a cation/proton antiporter found in *Staphylococcus aureus* (Chin et al., 2015). Based on a DRaCALA assay, it is known that c-di-AMP binds to SaCpaA. SaCpaA and YjbQ are orthologous proteins that share 52% of sequence homology according to Subtiwiki. Similarly to SaCpaA, YjbQ has an RCK domain in its C-terminus, supporting the proposal for a role of YjbQ in K+ transport (Fahmi et al., 2017) and it has been shown that just like KhtTU, YjbQ binds c-di-AMP (Gundlach et al., 2019). Previous unpublished research from Marta Gomes in our laboratory, confirmed that c-di-AMP binds to the C-terminal RCK domain of YjbQ by determining its structure (Figure 5). Importantly, it has been proposed that c-di-AMP activates K+ transport in YjbQ. However, the current published data regarding the functional and structural properties of YjbQ is limited. Thus, further work is necessary to achieve a better understanding about the functional properties of this transporter, in particularly concerning the role of c-di-AMP on its function.
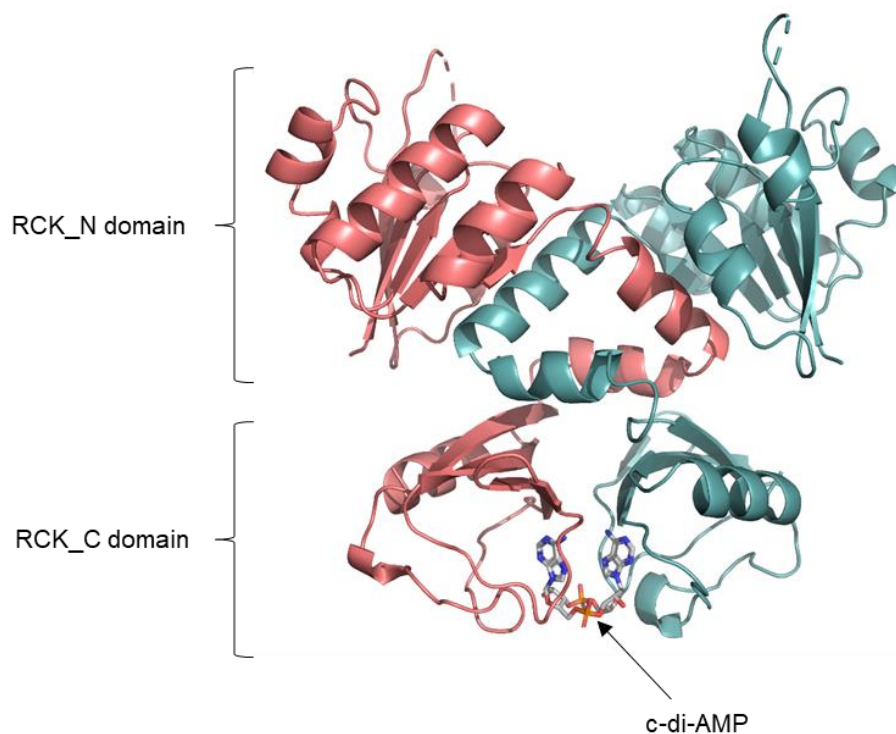
Figure 5: Structure of the RCK domain of YjbQ, with c-di-AMP binding at the interface of two RCK_C domains. Each subunit is represented in a different color. The N and C domains of one of the subunits are indicated. This image was created with PyMOL using unpublished data from Marta Gomes.

2.Objectives

The main goal of this work is to determine the functional properties of YjbQ. We want to gain a better understanding of the ion transport mechanism by answering the following questions, namely: how is the activity of YjbQ affected by variations in pH? Is YjbQ selective for K^+ or does it also transport other cations? Since it has been previously shown that c-di-AMP is a ligand of the RCK_C subdomain of YjbQ, how does that interaction interfere with the activity of this transporter? Does the presence of YjbQ contribute to growth of *Bacillus subtilis* in acidic and/or alkaline environmental conditions?

In order to obtain answers to these questions, I used a fluorescence-flux based assay with everted vesicles to test ionic selectivity, and detect activity differences with pH and c-di-AMP concentrations. Additionally, *Bacillus subtilis* growth assays were performed in different potassium concentrations and pH, with and without expression of YjbQ.

3. Materials and methods

3.1 Media and strains

Liquid media was prepared as described in Table 1 and later autoclaved at 121 °C. To produce solid media (plates with or without antibiotics) 15 g/L of agar was added to the liquid media before sterilization. The main strains used in this work are presented in Table 2.

Table 1: List of ingredients for preparation of different media used in this work

Media	Composition
LB (Lysogeny Broth)	10 g/L tryptone, 5 g/L yeast extract, 10 g/L NaCl
LB-BS (Lysogeny Broth adapted for *Bacillus subtilis*)	10 g/L tryptone, 5g/L yeast extract, 5 g/L NaCl
LBK (Lysogeny Broth with K⁺)	10 g/L tryptone, 5 g/L yeast extract, 10 g/L KCl
LBK-BS (Lysogeny Broth with K⁺ adapted for *Bacillus subtilis*)	10 g/L tryptone, 5 g/L yeast extract, 5 g/L KCl
SMM (Spizizen Minimal Medium)	2 g/L $(NH_4)_2SO_4$, 1 g/L $Na_3C_6H_5O_7.2H_2O$, 0.246 g/L $MgSO_4.7H_2O$, 0.5% glucose, 50 mg/L tryptophan, 50 mg/L phenylalanine, trace elements (125 mg/L $MgCl_2.6H_2O$, 7.3 mg/L $CaCl_2.2H_2O$, 13.5 mg/L $FeCl_2.6H_2O$, 1 mg/L $MnCl_2.4H_2O$, 1.7 mg/L $ZnCl_2$, 0.43 mg/L $CuCl_2.2H_2O$, 0.3 mg/L $CoCl_2$ and 0.6 mg/L $NaMoO_4.2H_2O$), and K_2HPO_4, KH_2PO_4, Na_2HPO_4 and NaH_2PO_4 in varying proportions so that $[K^+]+[Na^+] = 150$ mM and $[HPO_4^{2-}]/[H_2PO_4^-] = 2$ (pH 7.0)
YPD (Yeast extract, Peptone, Dextrose)	10 g/L yeast extract, 20 g/L peptone, 20 g/L dextrose (+ added KCl and 100 mM buffer depending on experimental conditions)

GM1	2 g/L $(NH_4)_2SO_4$, 14 g/L K_2HPO_4, 6g/L KH_2PO_4, 1 g/L $Na_3C_6H_5O_7.2H_2O$, 0.81 mM $MgSO_4.7H_2O$, 0.9% glucose, 50 mg/L tryptophan, 50 mg/L phenylalanine, trace elements (125 mg/L $MgCl_2.6H_2O$, 7.3 mg/L $CaCl_2.2H_2O$, 13.5 mg/L $FeCl_2.6H_2O$, 1 mg/L $MnCl_2.4H_2O$, 1,7 mg/L $ZnCl_2$, 0.43 mg/L $CuCl_2.2H_2O$, 0.6 mg/L $CoCl_2$, 0.6 mg/L $NaMoO_4.2H_2O$), 0.1% bacto-yeast extract, 0.02% bacto-casaminoacids
GM2	2 g/L $(NH_4)_2SO_4$, 14 g/L K_2HPO_4, 6g/L KH_2PO_4, 1 g/L $Na_3C_6H_5O_7.2H_2O$, 0.81 mM $MgSO_4.7H_2O$, 0.9% glucose, 50 mg/L tryptophan, 50 mg/L phenylalanine, trace elements (125 mg/L $MgCl_2.6H_2O$, 7.3 mg/L $CaCl_2.2H_2O$, 13.5 mg/L $FeCl_2.6H_2O$, 1 mg/L $MnCl_2.4H_2O$, 1,7 mg/L $ZnCl_2$, 0.43 mg/L $CuCl_2.2H_2O$, 0.6 mg/L $CoCl_2$, 0.6 mg/L $NaMoO_4.2H_2O$), 0.1% bacto-yeast extract, 0.02% bacto-casaminoacids, 0.5 mM $CaCl_2$, 2.5 mM $MgCl_2$

Table 2: Information regarding the genotype of the main strains used in this work

Strain	Genotype
NEB 5-alpha (*Escherichia coli*)	fhuA2Δ(argF-lacZ)U169 phoA glnV44 Φ80 Δ(lacZ)M15 gyrA96 recA1 relA1 endA1 thi-1 hsdR17 (*Biocompare: The Buyer's Guide for Life Scientists*, n.d.)
Knabc (*E. coli*)	ΔnhaA ΔnhaB ΔchaA (Nozaki et al., 1996; Shao et al., 2018)
168 (*Bacillus subtilis*)	trpC2 (Albertini & Galizzi, 1999)

3.2 Molecular biology

3.2.1 Site-directed mutagenesis

Mutation oligonucleotides (primers) were designed with the QuikChange Primer Design server from Agilent to mutate residues in the RCK_C subdomain of YjbQ, histidine to alanine in position 585 (H585A) and arginine to alanine in position 589 (R589A). With these primers, a polymerase chain reaction (PCR) was performed to amplify the DNA template, the pBAD-*yjbQ* construct previously generated in the lab. The

non-mutated template was digested during 2 hours at 37 ºC in a Thermomixer (Eppendorf) by adding to the PCR mixture the DpnI restriction enzyme (Thermo Scientific). DpnI recognizes methylated nucleotides found in naturally occurring DNA material, as opposed to the non-methylated amplified DNA. The resulting digestion product was transformed into NEB 5-alpha competent cells, which were plated in LB solid medium with the appropriate antibiotics and incubated overnight at 37 ºC in a Lab-Line Imperial Incubator III. Four colonies were inoculated in liquid medium with antibiotics and grown overnight at 37 ºC, with 220 rpm agitation, in an I-2400 Digital Incubator Shaker (New Brunswick Scientific). These cultures were centrifuged and two of them were used for plasmid DNA purification with the NZYMiniprep Kit (NZYtech), and later sent for sequencing at Eurofins Genomics, to ensure that the proper mutations were present. Primers utilized in the mutagenesis protocol are shown in Table 3.

Table 3: Primers designed to create mutants of *yjbQ*

Construct:	Vector:	Insert:	Oligos*:
pBAD-*yjbQ*(H585A)	pBAD_{His b} (resistance to ampicillin in *E. coli*)	*yjbQ* mutated (H585A)	Forward: 5'-GTGTGGACAGCATCG TTCCT**GCA**GGGGATA CGAGGC-3' Reverse: 5'-GCCTCGTATCCCCTG CAGGAACGATGCTGT CCACAC-3'
pBAD-*yjbQ*(R589A)	pBAD_{His b} (resistance to ampicillin in *E. coli*)	*yjbQ* mutated (R585A)	Forward: 5'-TTCCTCATGGGGATA CG**GCG**CTGAAACTTG GAGACC-3' Reverse: 5'-GGTCTCCAAGTTTCA GCGCCGTATCCCCAT GAGGAA-3'

*Mutation codon is shown in bold.

3.2.2 Cloning with restriction enzymes

For cloning in pBAD plasmid, the *yjbQ* orthologous genes from the species *Mesobacillus foraminis*, *Metabacillus litoralis*, and *Staphylococcus aureus* were amplified by PCR from genomic DNA. Alternatively, the pBAD-*yjbQ* construct was used as a template for the amplification of *yjbQ* as the insert for cloning into the pBS0E plasmid. The resulting PCR products were analyzed by 1%(w/v) agarose gel electrophoresis (with TAE buffer) to confirm the presence of a DNA fragment with the expected molecular weight. The fragments were purified using the QIAquick PCR Purification Kit (QIAGEN). Then, both the plasmid (pBAD or pBS0E) and the amplified gene were digested during 3 hours at 37 ºC in a Thermomixer (Eppendorf) with restriction enzymes that targeted specific restriction sites, mentioned in Table 4. The digested PCR fragments and plasmid were further purified in a 1%(w/v) agarose gel electrophoresis (with TAE buffer). While avoiding UV radiation exposure to decrease DNA alterations, the agarose gel was cut to obtain the bands of the PCR fragment and plasmid. The DNA was extracted from the gel bands using the NZYGelpure Kit (NZYtech). The resultant purified products were mixed in a 7:1 or 16:1 proportion of insert/plasmid together with T4 DNA ligase and ligase buffer, and went through a ligation reaction at 4 ºC overnight. The product of ligation was transformed into NEB 5-alpha competent cells, which were plated on LB plates with antibiotics and incubated overnight at 37 ºC in a Lab-Line Imperial Incubator III. From the colonies that grew on the plate, 10 were selected to be inoculated in liquid medium in test tubes with antibiotics and grown overnight at 37 ºC, with 220 rpm agitation, in a I-2400 Digital Incubator Shaker (New Brunswick Scientific). A Bacterial Colony PCR protocol was performed in a small fraction (100 µL) of the overnight culture, which involved cellular lysis to release plasmid DNA and PCR amplification with primers that anneal at the inserted gene, therefore allowing the identification of colonies that contained the clone of interest. From the positive overnight growths, two were selected and plasmid DNA was prepared from them, using the NZYMiniprep Kit (NZYtech), that would later be sequenced by Eurofins Genomics, to confirm that no significant mutations were present.

Table 4: Primers used for cloning *yjbQ* and its orthologs

Construct:	Vector:	Insert:	Oligos*:
pBAD-EV146_101175	pBAD_{His b} (resistance to ampicillin in *E. coli*)	EV146_101175 (*yjbQ* ortholog from *M. foraminis*)	Forward: 5'-TGACTA**CCATGG**AA CAGCATGGTTCC ATTATG-3' (Ncol) Reverse: 5'-GAATTT**GGTACC**TTA ATACCATCTGCC- 3' (Kpnl)
pBAD-A6K24_06980	pBAD_{His b} (resistance to ampicillin in *E. coli*)	A6K24_06980 (*yjbQ* ortholog from *M. litoralis*)	Forward: 5'-GATTTA**CCATGG**TGA TGCATGGTGCATCCG TAACTTCATTAG-3' (Ncol) Reverse: 5'-GAATTT**GGTACC**TTA GATAAGCTCAAG-3' (Kpnl)
pBAD-*cpaA*	pBAD_{His b} (resistance to ampicillin in *E. coli*)	*cpaA* (*yjbQ* ortholog from *S. aureus*)	Forward: 5'-GAATTT**CCATGG**AGT TTTTATCTTTAGTTA-3' (Ncol) Reverse: 5'-GAATTT**GGTACC**TTA AAAATAAAATTC-3' (Kpnl)
pBS0E-*yjbQ*	pBS0E (resistance to ampicillin in *E. coli* and to lincomycin and erytromycin in *B. subtilis*)	*yjbQ* (*B. subtilis*)	Forward: 5'-AGTACA**TCTAGA**TAA GGAGGAACTACTATGGCG CATACATCTGTC-3' (Xbal) Reverse: 5'-GCCTAA**CCATGG**TTAT CCTTCCAATGTT TTC-3' (Ncol)

*Restriction sites are shown in bold and indicated in parenthesis.

3.2.3 Transformation of *E. coli* and *B. subtilis*

Transformation in *E. coli* involved a first step of transferring 1-7µL of plasmid into 100 µL of competent cells, followed by an incubation on ice for 30 minutes, then a heat shock at 42 ºC for around 40 seconds. The Eppendorf tubes with competent cells were put on ice for another 2 minutes before 900µL of LB or LBK was added. Next, cells were incubated at 37 ºC for 1 hour at 220 rpm in a I-2400 Digital Incubator Shaker (New Brunswick Scientific). At the end of this step, a centrifugation at 5000 rpm for 1 minute was carried out. A large part of the supernatant was removed, and the pellet was resuspended in the remainder and plated on a LB or LBK plate with appropriate antibiotics. Plates were incubated overnight at 37 ºC in a Lab-Line Imperial Incubator III.

For the protocol of transformation in *B. subtilis*, cells from glycerol stocks were streaked on LB-BS or LBK-BS agar plate with an inoculation loop and incubated at room temperature for some days or overnight at 37 ºC in a Lab-Line Imperial Incubator III, placed. From this plate, colonies were inoculated into 5 mL of pre-heated GM1 medium in a 100 mL Erlenmeyer flask and incubated at 37 ºC and 180 rpm for 5 hours in a Multitron (INFORS HT). Then, 1 mL of cellular culture was transferred to another 100 mL Erlenmeyer flask together with 4 mL of pre-heated GM2 medium, and incubated in the same conditions for 2 hours. From this flask, 500 µL of cells were transferred to test tubes where approximately 10-15 µL of PCR product or plasmids had been previously added. The same operation was performed into tubes without DNA as a negative control. Tubes were incubated at 37 ºC and 180 rpm for 1 hour in a I-2400 Digital Incubator Shaker (New Brunswick Scientific). After a centrifugation at 3000 rpm for 3 minutes, part of the supernatant was discarded, and the pellet was resuspended in the remaining volume of supernatant for plating on LB-BS or LBK-BS plates with the appropriate antibiotics. Plates were incubated overnight at 37 ºC in a Lab-Line Imperial Incubator III, or at room temperature.

3.3   Production of everted membrane vesicles

pBAD-*yjbQ* and pBAD33-DAC were co-transformed in competent KNabc strain, which lacks major antiporters (mentioned in Table 2), and plated on LBK solid medium, that contained antibiotics for selection of plasmids in *E. coli*: ampicillin for pBAD-*yjbQ* and chloramphenicol for pBAD33-DAC to the final concentrations of 100 µg/mL and 35 µg/mL, respectively. Plates were incubated overnight at 37 ºC in a Lab-Line Imperial Incubator III.

Colonies grown in lawn in the agar plates were resuspended in 5 mL of LBK media and transferred to a final volume of 1 L of LBK, with ampicillin and chloramphenicol at 100 μg/mL and 35 μg/mL. Each plate was sufficient for 2 L culture, with 1 L of growth medium in a 4 L Erlenmeyer. Cultures were grown at 37 °C and 130 rpm in a Multitron (INFORS HT), until they reached an OD value, measured in an Ultrospec 10 Cell Density Meter (Amersham Biosciences), around 0.8. At that moment, protein expression was induced with 0.002% L-arabinose and cultures were then left growing overnight at 30 °C. Cell pellets were collected by centrifugation at 5000xg during 10 minutes (4 °C) in a Beckman Avanti J-26XP high speed centrifuge, and then frozen at -20 °C.

Stock solutions of sucrose (1M), DTT (1M), choline chloride (1M) and HEPES pH 7.0 (1M) were prepared beforehand in Type I water and filtered. On the day of the preparation of everted vesicles, the collected pellets were unfrozen by immersion in a beaker of water at room temperature. A solution with buffer for vesicles, "Vesicle Buffer", was prepared from the stock solutions to the final concentrations of 20 mM HEPES pH 7.0, 140 mM choline chloride, 0.5 mM DTT and 250 mM sucrose with Type I water. Pellets were resuspended in this buffer to homogeneity using a pipette and then centrifuged in a Beckman Avanti J-26XP high-speed centrifuge at 5000xg, 4 °C for 20 minutes, in pre-weighed centrifugation tubes. The resulting supernatant was discarded, and the weight of the pellets, relevant for a later step, was recorded. Pellets were resuspended in Vesicle Buffer solution to 35 mL, which is the maximum volume to fill the cell of the French Press. Cells were lysed by a single passage at approximately 4000 psi. Then, samples were incubated at room temperature with MgCl$_2$ and DNAse at final concentrations of 10 mM and 20μg/mL, respectively. This was followed by a 5000xg centrifugation to remove cells that were not lysed. The supernatant containing the membrane vesicles was carefully removed, to avoid contamination from the soft pellet, and transferred to ultracentrifugation tubes until full capacity. A subsequent centrifugation in a Beckman Optima L-80 XP Ultracentrifuge at 100,000xg for 1 hour and 10 minutes took place so that the membrane vesicles were pelleted and the supernatant was discarded. The pellet was resuspended in Vesicle Buffer solution and centrifuged again at 100,000xg to further clean the sample. Finally, the resulting vesicles were resuspended in Vesicle Buffer solution at 1 g/ml of the original pellet weight, frozen with liquid nitrogen and stored at -80 °C.

To produce everted vesicles lacking YjbQ (empty vesicles), the same procedure took place but with Knabc cells transformed with pBAD and pBAD33 plasmids without inserts. To study the *M. foraminis* and *M. litoralis* orthologs of *yjbQ*, vesicles were produced from

cells transformed with the transporter constructs but without pBAD33-DAC, while for *cpaA* from *S. aureus*, cells were transformed with and without the DAC domain.

For each everted vesicle preparation, the total protein concentration was determined with Bradford reagent and a calibration curve determined with BSA (Bovine Serum Albumin) as a standard.

3.4 Fluorescence-flux based activity assays

Antiporter activity was measured using an *in vitro* fluorescence-based flux assay. Everted vesicles were resuspended at a total protein concentration of 133 µg/mL in a buffer solution containing 15 mM Tris-HCl buffer at different pH values, 140 mM choline chloride and 5 mM $MgCl_2$. The fluorescent probe, ACMA (9-amino-6-chloro-2-methoxyacridine), was added to a final concentration of 2 µM and incubated for 3 minutes at room temperature in the dark, before starting the fluorescence measurements in a HORIBA FluoroMax-4 spectrofluorometer. For the assay, the vesicle solution in the cuvette was kept at room temperature and subjected to constant stirring with a magnetic bar. Fluorescence measurements were performed with the following setup: excitation wavelength at 410 nm, emission wavelength at 480 nm, 2 nm slits and integration rate of 0.2 seconds. Vesicles were incubated for 50 seconds in the cuvette before addition of lactate to a final concentration of 4 mM. This resulted in the charging of H^+ into the lumen of the vesicles through oxidation of lactate by the lactate dehydrogenase present in the *E. coli* membrane, and fluorescence quenching. This was followed by addition of a salt that contained the cation of interest at around the 200 seconds, resulting in fluorescence dequenching as protons and cation are exchanged by the antiporter. For assays involving c-di-AMP, varying concentrations of the dinucleotide resuspended in Tris-HCl, were added just before lactate.

The fluorescence data were processed with Origin 8.5 (Origin Lab).

3.5 Generation of a *Bacillus subtilis* mutant strain that lacks *yjbQ*

The *Bacillus subtilis* strain lacking *yjbQ*, 168*ΔyjbQ (ΔyjbQ::kan)*, in which *yjbQ* was replaced with a kanamycin resistance cassette, was acquired from *Bacillus* Genetic Stock Center. The strain was streaked on LB-BS or LBK-BS agar plates (with kanamycin) and incubated in the dark at room temperature over two to five days or at 37 ºC overnight

in a Lab-Line Imperial Incubator III. Colonies were inoculated in liquid medium with kanamycin and cultures grown at 37 ºC overnight, with 220 rpm agitation, in a I-2400 Digital Incubator Shaker (New Brunswick Scientific). From this culture, part was mixed with glycerol (for a final concentration of 20%), frozen in liquid nitrogen and stored at -80 ºC.

To generate the 168*ΔyjbQ* strain in the background of our laboratory strain 168 (to avoid variations between 168 strains of different origins), we purified genomic DNA from the purchased 168*ΔyjbQ* culture by following the instructions from the GeneJET Genomic DNA Purification Kit (Thermo Fisher). Purified genomic DNA was used as a template to amplify by PCR the kanamycin cassette together with *B. subtilis* DNA flanking regions. Primers shown in Table 5 anneal to sequences within the 168 genome positioned ~600 nucleotides down-stream and up-stream from the 5´ and 3´ ends of the kanamycin cassette, respectively. These regions are essential for promoting homologous recombination after transformation in our lab 168 strain. The PCR product was purified in 1%(w/v) agarose gel electrophoresis (with TAE buffer), the band fragment cut and DNA isolated with the NZYGelpure Kit (NZYtech). The purified product was transformed into the laboratory *Bacillus subtilis* 168 and plated on LBK-BS agar plates with kanamycin. Colonies that grew were inoculated in liquid medium with kanamycin and grown overnight at 37 ºC. From these tubes, part was used to create glycerol stocks and part was used to confirm the presence of the kanamycin cassette replacing *yjbQ* by purifying genomic DNA and performing a PCR with the same primer pair in the mutant strains and laboratory 168 strain, followed by analysis in a 1%(w/v) agarose gel electrophoresis (with TAE buffer).

Table 5: Primers designed for regions around *yjbQ* in the genomic DNA from *Bacillus subtilis*

Oligos:	Description:
Forward: 5'-ACAAAGTCCTTCACTCTGCGGGTATATTTGCCGATATC-3' Reverse: 5'-GATGACAAAATTCTCTTTCATCTTGGCACGCACTTC-3'	Primers that reach around 600 nucleotides upstream and downstrem *yjbQ* in the genomic DNA sequence of *Bacillus subtilis*.

3.6   Generation of a *B. subtilis* strain over-expressing YjbQ

The pBS0E plasmid was used for over-expression of YjbQ in *B subtilis* upon induction with bacitracin. Empty pBS0E plasmid and the pBS0E-*yjbQ* plasmid were transformed into one of the 168Δ*yjbQ (ΔyjbQ::kan)* mutant strains generated above. The resulting strains either contained *yjbQ* in pBS0E plasmid, 168Δ*yjbQ* (pBS0E-*yjbQ*), or the empty version of pBS0E plasmid, 168Δ*yjbQ* (pBS0E); these strains were selected on LBK-BS plates with kanamycin, lincomycin and erythromycin. Colonies were streaked onto new plates of the same kind, grown, inoculated in liquid LBK-BS with antibiotics, and glycerol stocks were prepared from these cultures.

3.7   Growth assays with *Bacillus subtilis*

Bacillus subtilis growth assays were performed in media supplemented with antibiotics, containing different potassium concentration and varying pH values. Firstly, cells from different strains were streaked on LBK-BS agar plate, with or without antibiotics according to the strain, and incubated overnight at 37 ºC in a Lab-Line Imperial Incubator III.

Preliminary tests with two types of media, SMM and YPD, with different K^+ concentrations (0.5 mM and 100 mM) and different pH values (5.5, 7.5 and 9.0 with YPD media (in 24-well plates), and 7.0 with SMM (in test tubes), were done in a Multitron (INFORS HT) incubator, with OD measurements in an Ultrospec 10 Cell Density Meter (Amersham Biosciences).

Final growth experiments with technical replicates were performed in 96-well plates. For experiments with SMM at pH 7.0, *B. subtilis* strains 168, 168Δ*yjbQ*, 168Δ*yjbQ* (pBS0E) and 168Δ*yjbQ* (pBS0E-*yjbQ*) were grown in pre-cultures (5 mL) with SMM 40 mM K^+, with no antibiotics in the case of strain 168 alone, with 7.5 µg/mL kanamycin, 25 µg/mL lincomycin and 1 µg/mL erythromycin (for strains transformed with pBS0E plasmid), or with 7.5 µg/mL kanamycin in the case of the strain 168Δ*yjbQ*, at 37 ºC and 180 rpm for 9 hours. Cultures with a final volume of 100 µL were inoculated in a 96-well plate at a starting $OD_{600\,nm}$ ~0.05 in SMM media supplemented either with 0.5 mM K^+ or 100 mM K^+, with antibiotics and 30 µg/mL bacitracin to induce protein expression. Growths were carried out in a Synergy Mx Microplate Reader (BioTek) overnight at 37 ºC for around 14-15 hours with medium agitation, with automatic OD measurements done every 30 minutes.

For experiments at pH 5.5 and 9.0, growths were carried out in YPD medium that included 100 mM buffer, either Bis-tris propane at pH 9.0 or MES at pH 5.5, with 100 mM KCl, 2 mM KCl or 0.5mM KCl, antibiotics and bacitracin as described above. Cells were resuspended from plates into YPD with low K^+, OD was measured and an intermediate dilution to OD 1.0 was performed in the same low K^+ medium. This was followed with a final dilution to OD ~0.05 in the final experimental liquid medium in a volume of 100 μL in a 96-well plate. Measurements were performed in a Synergy Mx Microplate Reader (BioTek) under the same conditions described above.

4. Results and Discussion

4.1   *In vitro* fluorescence-based flux assays from everted vesicles

4.1.1   Establishing growth conditions

Earlier experiments showed that upon induction of expression of YjbQ in the Knabc strain, cell cultures grew to lower ODs in the stationary phase, which might indicate a toxic effect of the protein. Therefore, preliminary tests for production of vesicles were done to set the best concentration of inducer and temperature throughout cell growth and expression of protein as well as to decide whether to include the DAC domain, which produces the putative regulatory ligand of YjbQ (c-di-AMP) in *E. coli* (Gundlach et al., 2019), possibly changing the protein impact on cell growth.

Figure 6 represents a preliminary test with pBAD-*yjbQ* in Knabc cells, with variations in temperature and arabinose concentrations. Cells were grown at 37 ºC until reaching an OD around 0.8-0.9. At this point, either 0.002% or 0.02% of inducer (L-arabinose) was added, and flasks were subjected to different temperatures of incubation (20 ºC, 25 ºC or 30 ºC) to change the rate of protein production and folding. After induction, cells grew better at the lower concentration of arabinose at all tested temperatures. When considering the lower concentration of inducer, the OD at the late-stage stationary phase is higher at lower temperatures, while at higher percentages of inducer, ODs are better at higher temperatures. The combination of 30 ºC and 0.002% arabinose seems to result in faster exponential phase growth and results in earlier stationary phase with high overnight OD.
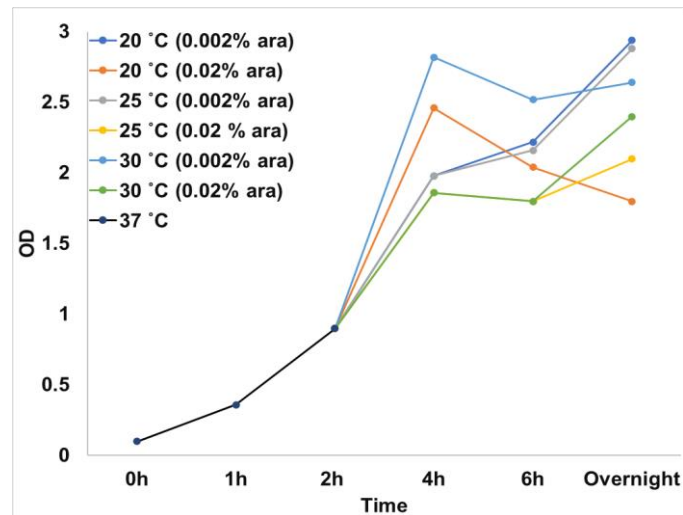
Figure 6: Exploring the impact of different inducer concentration and temperature on cell growth. Graph shows OD values at different time points of cell culture growth of the Knabc strain transformed with pBAD-*yjbQ* construct. Inoculation was done at OD ~0.1. Cells were shaken at around 200 rpm at 37 °C until OD ~0.9, induced with indicated amounts of arabinose (ara) and shifted to different incubation temperatures.

The 30 ºC condition was further explored in another test, shown in Figure 7, where the effect of the DAC domain was assessed. Three combinations of co-transformed plasmids were compared; pBAD-*yjbQ* together with pBAD33-DAC, pBAD-*yjbQ* and pBAD33 (empty), and pBAD (empty) together with pBAD33 (empty), as a negative control. From the growth curves, pBAD+pBAD33 pair showed the strongest growth, indicating that expression of YjbQ negatively affects cell growth, perhaps because more energetic resources have to be channeled for protein production (Diaz Ricci & Hernández, 2000; Wang et al., 2006). Between the other two conditions, differences are small and we decided to include the DAC domain.
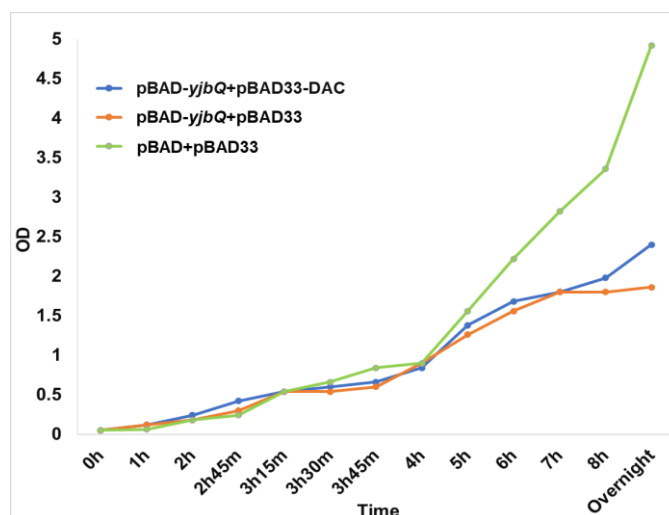
Figure 7: Exploring the impact of co-expression of YjbQ with the DAC domain on cell growth. Graph shows OD values at different points of cell culture growth of Knabc strain transformed with a combination of plasmids. Inoculation at OD=0.05. Cells were shaken at around 200 rpm at 37 °C until OD ~0.9, induced with 0.002% arabinose (ara) and shifted to 30 °C.

From these preliminary growth experiments, we settled on the following conditions to express YjbQ in the Knabc strain: co-expression with DAC domain, induction with 0.002% arabinose followed by incubation at 30 ºC overnight.

4.1.2 Flux assay and data processing

Everted vesicles were produced from Knabc cells expressing YjbQ and antiporter activity was measured using the *in vitro* fluorescence-based flux assay described in the methods section. The assay works in the following way. Vesicles are incubated with ACMA, a fluorescent dye that is sensitive to changes in proton gradient across the vesicle membrane. Lactate is added to the vesicles, activating the electron transport chain that generates a proton gradient by pumping protons into the vesicle lumen and therefore, quenching ACMA fluorescence (Figure 8). As fluorescence reaches a plateau, the cation of interest is added. If antiport occurs, then there is an increase in fluorescence intensity as the exchange of protons and cations dissipates the H^+ gradient, resulting in fluorescence dequenching. Crucially, the rate of dequenching is a related to the rate of transport or activity of the transporter.
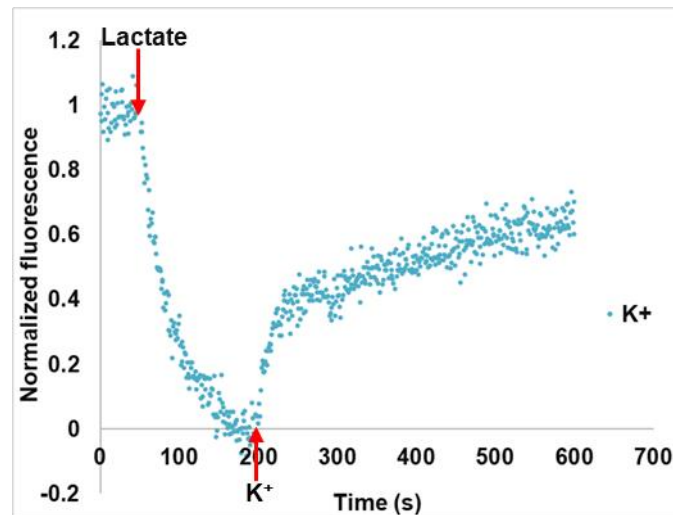
Figure 8: Normalized fluorescence recording with everted vesicle ACMA flux assay. Addition of lactate and of K$^+$ are indicated and result in quenching and dequenching of ACMA fluorescence as the proton gradient is built and dissipated, respectively.

For direct comparison of data collected from different assays, the fluorescence data was normalized, as in Figure 8, according to the following formula: Normalized Fluorescence = (F-Fmin)/(Fmax-Fmin), in which F stands for fluorescence at a given moment, Fmin corresponds to minimum value of recorded fluorescence and Fmax to maximum of fluorescence.

Recordings clearly showed what appears to be dequenching after addition of K$^+$ (as KCl) (Figure 8). However, the curves are noisy, as can be seen in Figures 8 and 9, and we had difficulty in fitting exponential functions to extract dequenching rate constants, as initially planned. The graph in Figure 9 illustrates a comparison between several normalized curves collected in different conditions where multiple phases are detected in some curves after the addition of cation. These features raised the possibility that we were not observing K$^+$/H$^+$ antiport.
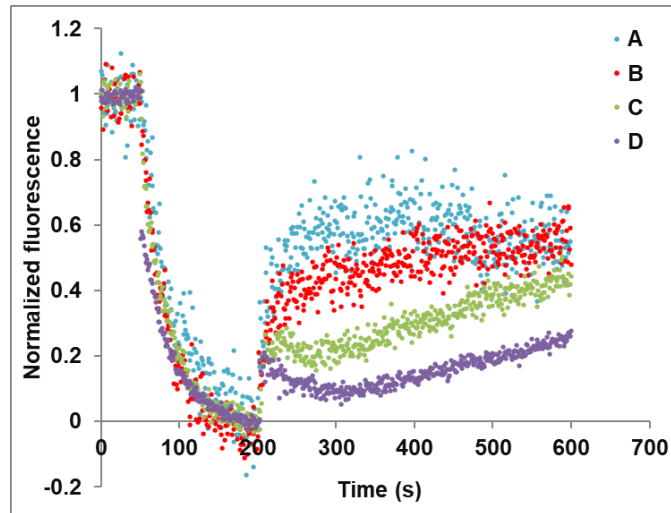
Figure 9: Comparison of normalized fluorescence curves of assays performed in different conditions. In particular, curve A has the expected shape, but curve B shows a rapid increase in fluorescence followed by a slow linear rise and curves C and D show three phases after addition of K^+, an initial jump in fluorescence, followed by a decrease and then a linear rise in fluorescence signal.

As a control, we collected data with addition of choline chloride. Choline$^+$ is an organic cation that is not transported by a K^+ transporter. We realized that the choline$^+$ curves should show any background features that are unrelated to K^+ transport; in particular, dissipation of the H^+ gradient by other proteins in the membrane of the vesicles. Therefore, we collected control data where we replaced K^+ for choline$^+$ and subtracted the choline$^+$ curves from each K^+ curve collected in identical conditions (Figure 10). These subtracted curves approach the expected flux curve shape and are reasonably fit by a single exponential in the rising phase immediately after addition of cation, giving us confidence that dequenching corresponded to K^+/H^+ antiport. However, the subtracted curves were still very noisy, and the rate constant values extracted from exponential fits varied widely between replicas.
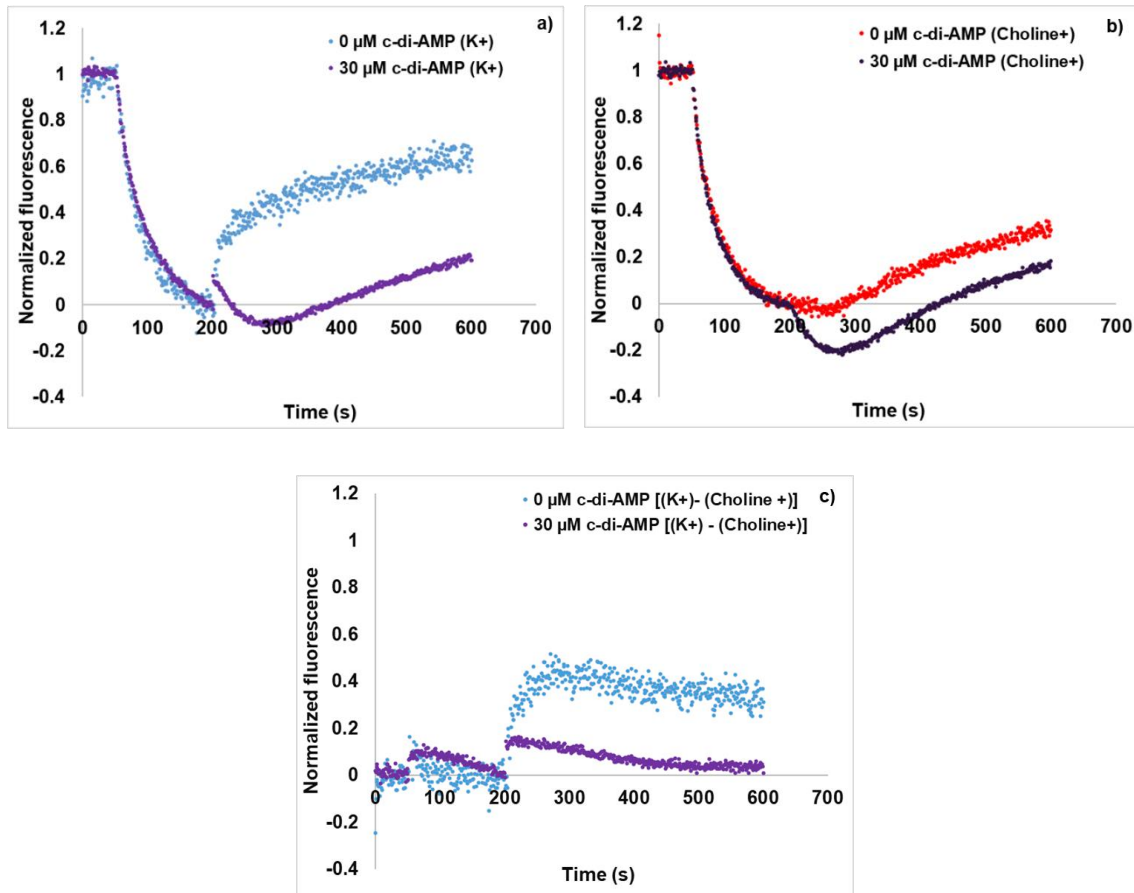
Figure 10: Correction of normalized K$^+$ flux curves; a) Normalized K$^+$ flux curves in two different conditions; b) Normalized choline$^+$ flux curves in the same conditions as in a). c) Corrected K$^+$ flux curves after subtracting fluorescence value from choline$^+$ assay in b) from fluorescence values in a).

Therefore, the data was processed using a different approach. Firstly, all the raw data curves were normalized according to the following approach: fluorescence values in a 11 sec interval just before addition of the cation (around 200 sec) were averaged, providing Fmin. The same was done to values before lactate addition, resulting in Fmax. After normalization, a reference point was selected at 400 seconds after the beginning of the assay, corresponding to 200 seconds after the moment of addition of the cation (see Figure 11). Due to high noise levels, we determined the value at 400 sec as the average of nearby points (from second "397" to second "403") for each curve. These 400 sec values were used to calculate averages and standard deviations between triplicates for each experimental condition. The final graphs and respective analysis are shown in the next subsections for each functional experiment that took place.

4.1.3 Ion transport selectivity

We were interested in determining if YjbQ was selective for K^+ over Na^+ as shown for KhtTU (Cereija et al, 2021). The selectivity assays were performed by changing the cation salt added at 200 seconds after the beginning of the measurement. Four cations (K^+, Na^+, Li^+ and Rb^+) were assessed, alongside choline$^+$ as a negative control (Figure 11).
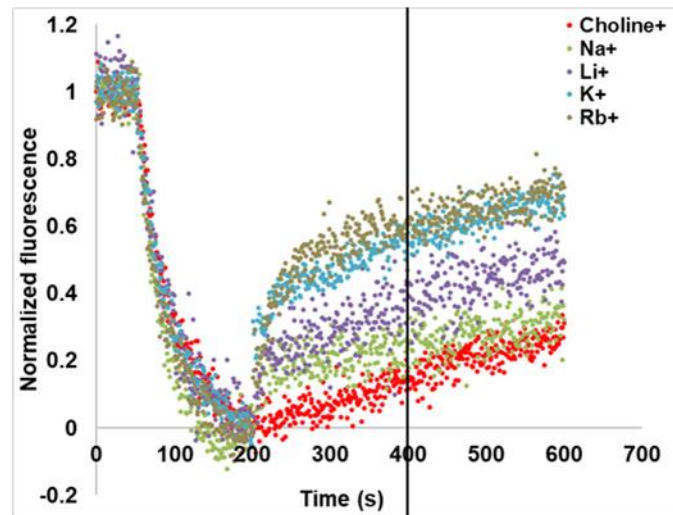

Figure 11: Comparison of normalized fluorescence flux curves for different cations (Choline$^+$, Na$^+$, Li$^+$, K$^+$, Rb$^+$). Fluorescence dequenching is more accentuated for K$^+$ and Rb$^+$ relative to Na$^+$ and Li$^+$.

Processed data from triplicates is shown in Figure 12. As one can see, fluorescence changes are larger for potassium and rubidium cations relative to sodium and lithium, indicating that YjbQ is more selective for the cations with larger radius. However, sodium and lithium still promote H^+ gradient dissipation over choline$^+$. Therefore, this data confirms that YjbQ is mainly a potassium transporter but that is not as highly selective as KhtTU.
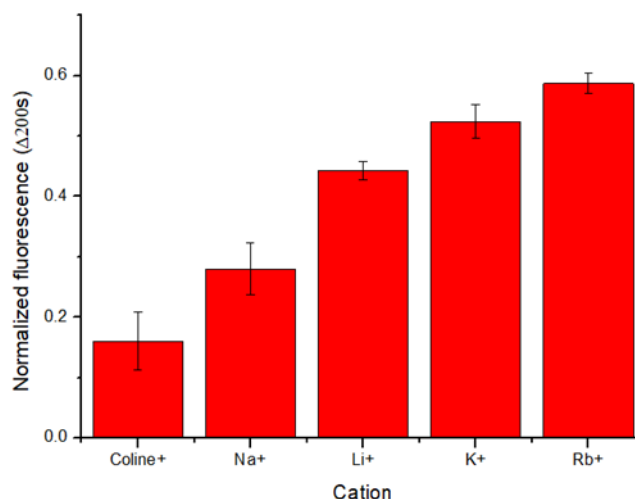
Figure 12: Bar chart of fluorescence changes for different cations (Choline[+], Na^{+}, Li^{+}, K^{+}, Rb^{+}). Averages and standard deviation are shown for triplicate measurements.

It has been noticed before that channels that select for potassium, also have a preference towards rubidium (Doyle et al., 1998), and those that select for sodium also show selectivity for lithium (Hille, 1972), though in both cases other ionic species may be allowed to flow through in a less significant manner. This effect occurs due to the similarity of ionic radii between these elements (Shrivastava et al., 2002). Therefore, our results from the selectivity assays go along what has been previously observed for other proteins. In terms of biological significance, it is important to retain the fact that YjbQ is more selective towards K^{+} while still transporting Na^{+}, since these two ions are present in high amounts in the bacterial environment.

4.1.4 pH dependence

To assess the pH dependence of YjbQ, fluorescence-based flux assays were carried out by adjusting the pH of the external buffer, which corresponds to the buffer bathing the cytosolic side of the membrane. Four different pH values were tested, 7.5, 8.0, 8.5 and 9.0 (Figure 13). Fluorescence dequenching after addition of K^{+} is more accentuated at higher pH levels with little or no change at pH 7.5.
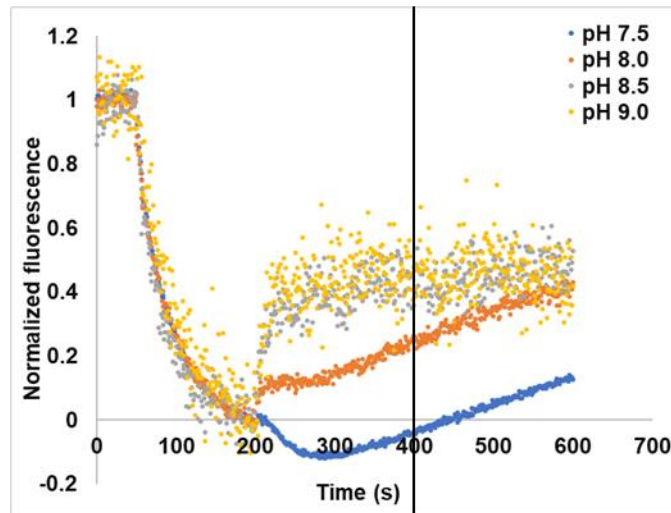
Figure 13: Comparison of normalized fluorescence flux curves measured in different external (cytosolic) pH conditions.

Plotting averages and standard deviations of all the triplicates (Figure 14) confirms increased transport of K$^+$ by YjbQ at higher pH values, which is in line with KhtTU and the role of K$^+$/H$^+$ antiporters in intracellular pH homeostasis against alkaline stress (Krulwich et al., 2011). It is worthwhile pointing out that noise increases with pH (Figure 13); therefore, there is no detectable difference between measurements at pH 8.5 and 9.0 (Figure 14). Thus, experiments were always performed at pH 8.5.
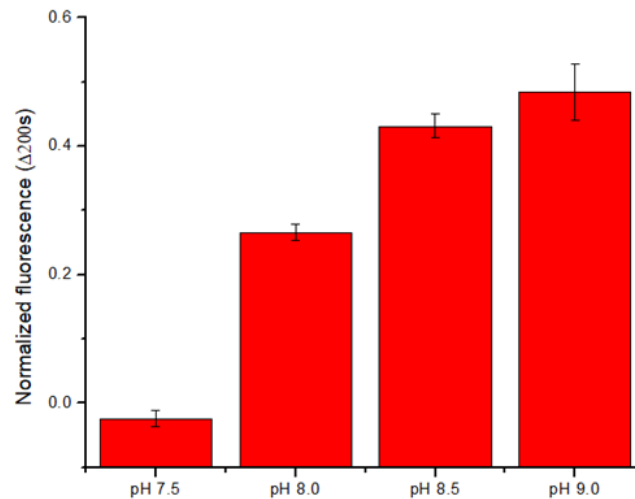

Figure 14: Bar chart of fluorescence changes for different pH values. Averages and standard deviation are shown for triplicate measurements.

4.1.5 c-di-AMP effect on the transport of K⁺

To assess the effect of c-di-AMP on K⁺ transport by YjbQ, dinucleotide titration experiments were conducted in the concentration range of 0 to 30 µM. In Figure 15, a flux curve measured in the presence of different c-di-AMP concentrations is displayed as an example, providing already a visual pattern of variation of measured fluorescence across tested c-di-AMP concentrations. The curve at the top corresponds to absence of added c-di-AMP and the curve at the bottom corresponds to maximum c-di-AMP concentration (30 µM). It is clear that there was a decrease in fluorescence dequenching, reflecting a decrease in K⁺/H⁺ antiport as the c-di-AMP concentration increased.
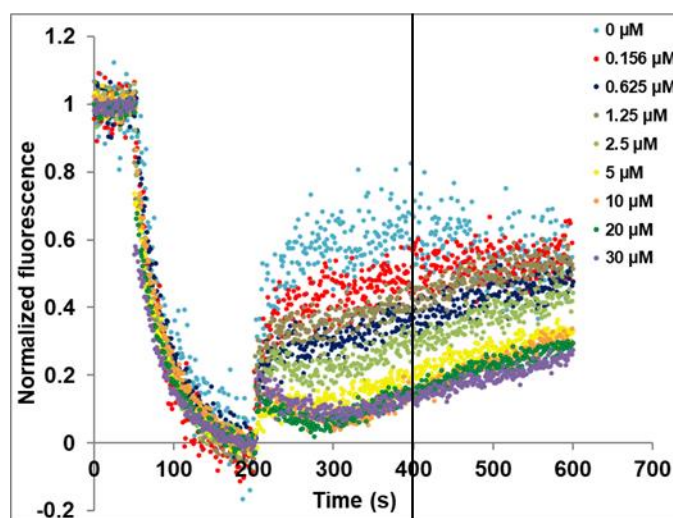
Figure 15: Comparison of normalized fluorescence flux curves measured for YjbQ in the presence of different c-di-AMP concentrations (0 µM, 0.156 µM, 0.625 µM, 1.25 µM, 2.5 µM, 5 µM, 10 µM, 20 µM and 30 µM).

Average fluorescence values (and standard deviation) were calculated from triplicates, normalized relative to fluorescence value at 0 µM and plotted in Figure 16. The data were fitted with a Hill equation ($y = \text{START} + (\text{END} - \text{START})(x^n/(K_{1/2}{}^n+x^n))$), where START is the normalized fluorescence value a 0 µM, END is the normalized fluorescence at very high concentrations of c-di-AMP, $K_{1/2}$ is the constant of 50% inactivation, n is the Hill coefficient. c-di-AMP inhibits YjbQ with a $K_{1/2} \sim 2$ µM.
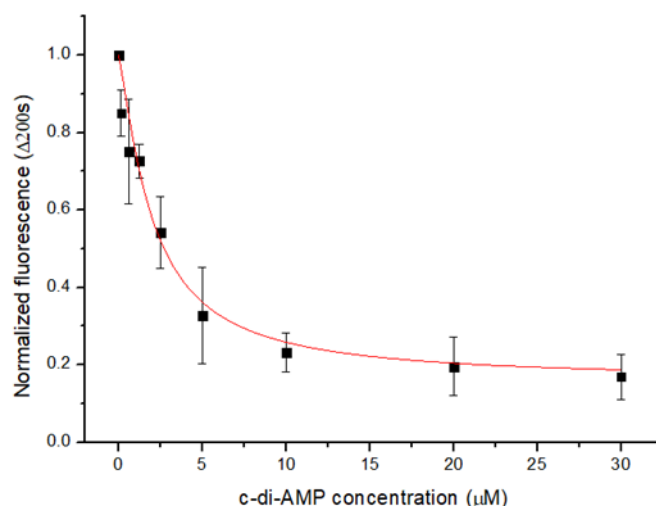
Figure 16: Plot of normalized fluorescence changes in the presence of increasing c-di-AMP concentrations. Averages and standard deviations of triplicate measurements were fitted with Hill equation. Start=1, End=0.16, K1/2= 2.0($\pm$0.3), n=1.25($\pm$0.20).

Contrary to expectations (Bai et al., 2014; Gibhardt et al, 2019; Gundlach et al., 2019; Gibhardt et al., 2020; Stülke and Krüger, 2020; Zarrella & Bai, 2020), YjbQ is inihibited by c-di-AMP. As mentioned in the introduction, transporters that promote export K^+, for example the *B. subtilis* KhtTU K^+/H^+ antiporter, have been shown to be activated by c-di-AMP binding, while transporters that import K^+, for example the *B. subtilis* KimA K^+/H^+ symporter, have been proposed to be inhibited by c-di-AMP binding. We are now showing that the impact of c-di-AMP in another K^+/H^+ antiporter does not fit this model. Since the physiological role of a protein is strongly determined by its regulation (when and where a protein is active or inactive) we need to consider whether YjbQ works as a K^+ importer. But before that, and because the measured signal for flux with YjbQ is relatively small and we have previously observed interference of c-di-AMP with the fluorescence properties of ACMA, we decided to gain further evidence that the c-di-AMP effect was in fact due to dinucleotide binding to YjbQ and to a change in YjbQ function.

One way to confirm that c-di-AMP in fact inhibits transport is to create mutants that affect its interaction with the protein. As previously mentioned, c-di-AMP binds at the RCK_C sub-domain. Therefore, we conducted an analysis of the conserved residues nearby the c-di-AMP binding pocket of the YjbQ RCK domain structure, determined in the laboratory. The conserved residue H585 was selected (Figure 17) because it participates in an apparently important set of interactions with the dinucleotide. It forms a hydrogen bond with a well-defined water molecule, which in turn interacts with an oxygen of a phosphate group and with an adenine from c-di-AMP. This is supported by

the measured distances between participating atoms, 2.7-3.3 Å, which are within the range expected for hydrogen bond interactions (McRee, 1999). Notably, it appears that, after c-di-AMP binding, this residue brings a certain level of closure of the RCK conformation to deter transportation. As a consequence, histidine 585 was mutated to alanine with the expectation that the $K_{1/2}$ of c-di-AMP would increase, demonstrating that we are monitoring the functional impact of c-di-AMP on YjbQ. Additionally, a non-conserved residue, R589 (Figure 17), which is located farther away from the active center, was also mutated to alanine. This mutation serves as a control experiment, showing that not every created mutant will increase the $K_{1/2}$ of inhibition.

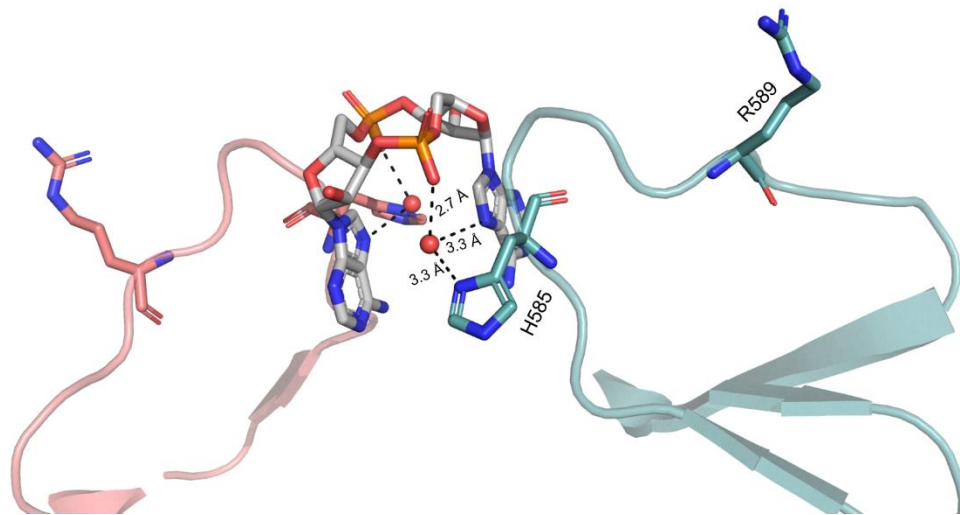**Figure 17:** Close-up view of the binding pocket of c-di-AMP in the RCK domain structure previously determined in the laboratory (unpublished). Subunits of the homodimer are shown in different colors. The intermolecular distances between c-di-AMP and the histidine residue and a nearby water molecule, corresponding to possible hydrogen bonds, are indicated in angstroms. The chosen residues for mutation, H585 and R589, are represented.
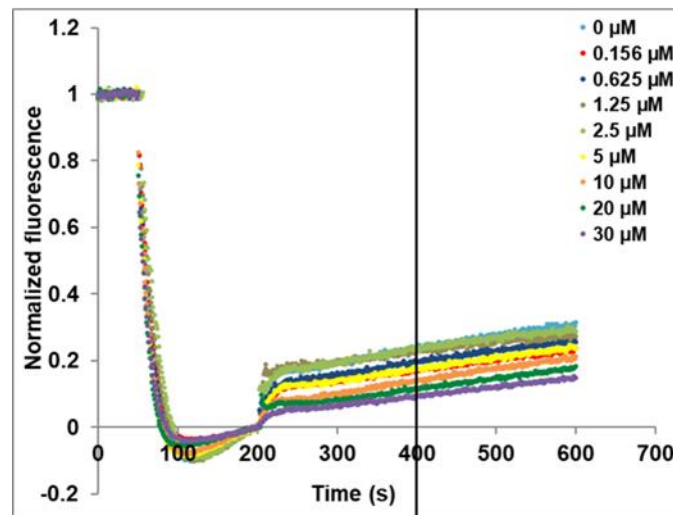
Figure 18: Comparison of normalized fluorescence flux curves for YjbQ-H585A measured in the presence of different c-di-AMP concentrations (0 µM, 0.156 µM, 0.625 µM, 1.25 µM, 2.5 µM, 5 µM, 10 µM, 20 µM and 30 µM).

We generated everted vesicles containing YjbQ-H585A and performed a c-di-AMP titration experiment, as described for the wild-type protein. The resulting fluorescence curves are shown Figure 18 and the processed data in Figure 19. The dequenching signal after addition of K^+ was smaller than with the wild-type protein but importantly, addition of c-di-AMP reduced dequenching. Plotting of average change in fluorescence with c-di-AMP concentration reveals a shallower dependence on c-di-AMP compared to the wild type, suggesting that c-di-AMP has less impact in YjbQ function. As expected, $K_{1/2}$ is shifted to a higher value, ~11 µM.

Figure 19: Plot of normalized fluorescence changes for YjbQ-H585A in the presence of increasing c-di-AMP concentrations. Averages and standard deviations of triplicate measurements were fitted with Hill equation. Start=1, End=0.16, K1/2= 11.3 (±0.8), n=1.04 (±0.08).

On the other hand, flux curves measured from everted vesicles with YjbQ-R589A showed a similar c-di-AMP dependence to wild-type YjbQ (Figure 20 and 21).
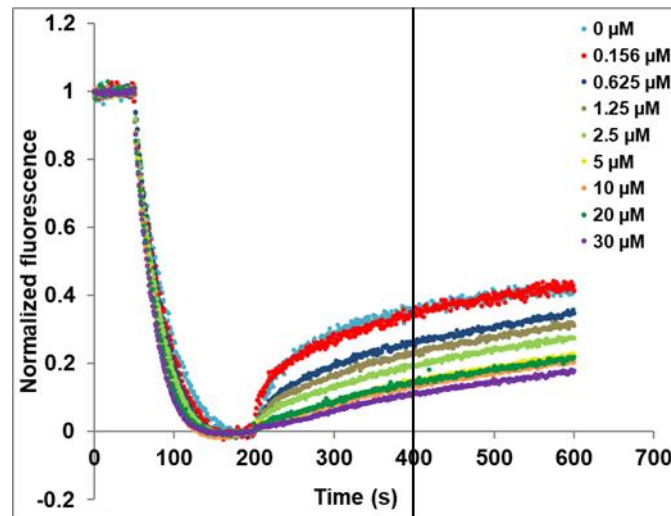
Figure 20: Comparison of normalized fluorescence flux curves for YjbQ-R589A measured in the presence of different c-di-AMP concentrations (0 µM, 0.156 µM, 0.625 µM, 1.25 µM, 2.5 µM, 5 µM, 10 µM, 20 µM and 30 µM).

In particular, the inhibitory effect of c-di-AMP was approximately the same, with a K1/2 value of ~1.4 µM. This result confirms that it is not just any mutant that will change the c-di-AMP dependence of YjbQ, strengthening the effect seen with the H585A mutation.
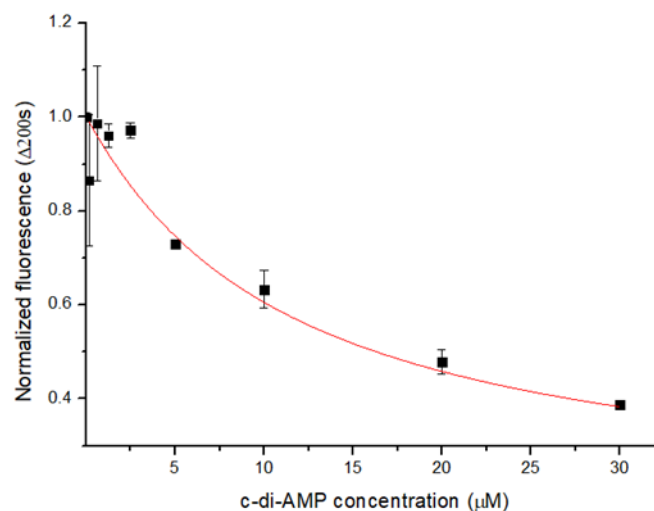

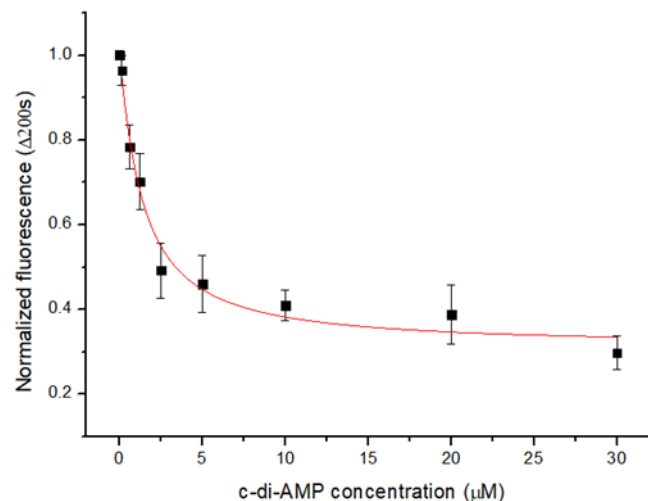**Figure 21:** Plot of normalized fluorescence changes for YjbQ-R589A in the presence of increasing c-di-AMP concentrations. Averages and standard deviations of triplicate measurements were fitted with Hill equation. Start=1, End=0.31, K1/2= 1.4 (±0.3), n=1.12 (±0.18).

Overall, we showed that c-di-AMP has an inhibitory effect on K^+/H^+ antiport by YjbQ. The concentration dependence of the effect is diminished by interfering with the binding pocket of the dinucleotide.

Taking into account that this inhibitory effect is contrary to what was expected, further experiments still need to be performed, particularly *in vivo*, to ensure that robust data sustain these observations. It is possible that the model that proposes that c-di-AMP inhibits K^+ importers and activates exporters is not strictly obeyed. Conversely, another hypothesis would be to explore the idea that YjbQ may function as a K^+ importer, rather than an exporter.

4.1.6 Empty vesicles

To further confirm that the observed flux curves correspond to transport by YjbQ, everted vesicles without YjbQ (or empty vesicles) were produced and tested. As expected, no transport was observed. Dequenching was not observed with either potassium, sodium, rubidium and choline cations (Figure 22). In addition, 10 µM c-di-AMP did not affect the fluorescence curve of K^+.

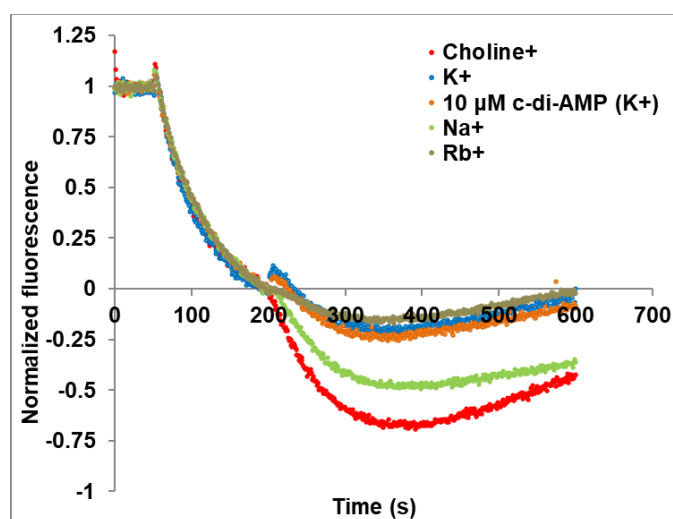**Figure 22:** Comparison of normalized fluorescence flux curves for empty vesicles measured in the presence of different cations (K^+, Na^+, Rb^+ and choline$^+$) as well as K^+ with 10 µM c-di-AMP.

4.1.7 YjbQ orthologous proteins

We selected three closely related orthologs of YjbQ with the goal of finding a protein with more robust flux activity but that share many of the functional properties of the *B.*

subtilis protein. We selected YjbQ orthologous proteins from *Mesobacillus foraminis*, *Metabacillus litoralis* and *S. aureus* with the amino acid sequence identities of 65%, 69% and 52%, respectively. *Mesobacillus foraminis*, *Metabacillus litoralis* and *B. subtilis* are all part of the same family, Bacillaceae. *S. aureus* belongs to a different family, Staphylococcaceae. Nonetheless, all of them belong to the same order of taxonomic classification, Bacillales (Schoch et al., 2020). The three genes were cloned as described in the methods section and everted vesicles were produced from Knabc cells expressing the proteins. Everted vesicles containing the ortholog from *M. foraminis* did not exhibit any activity when tested in the fluorescence assays in the same conditions used for YjbQ (Figure 23). In fact, fluorescence curves closely resemble those measured with empty vesicles (Figure 22).

Figure 23: Comparison of normalized fluorescence flux curves for vesicles prepared from Knabc cell expressing YjbQ orthologous protein from *Mesobacillus foraminis* measured in the presence of different cations (K^+, Na^+, choline$^+$).

Virtually the same results were observed in assays with everted vesicles generated from Knabc cells expressing the ortholog from *M. litoralis* (Figure 24).
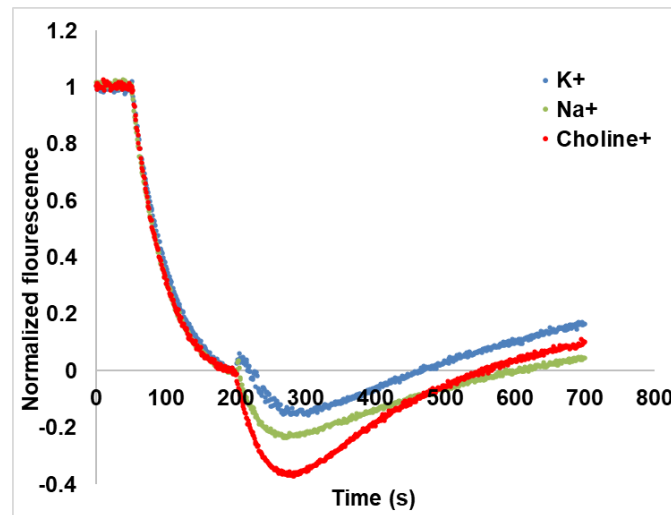
Figure 24: Comparison of normalized fluorescence flux curves for vesicles prepared from Knabc cell expressing YjbQ orthologous protein from *Metabacillus litoralis* measured in the presence of different cations (K$^+$, Na$^+$, choline$^+$).

With SaCpaA, the orthologous protein from *S. aureus*, everted vesicles were produced from cells co-transformed with and without the plasmid encoding the DAC domain. As shown in Figure 25, no activity was observed when vesicles were produced from cells that grew in either condition.
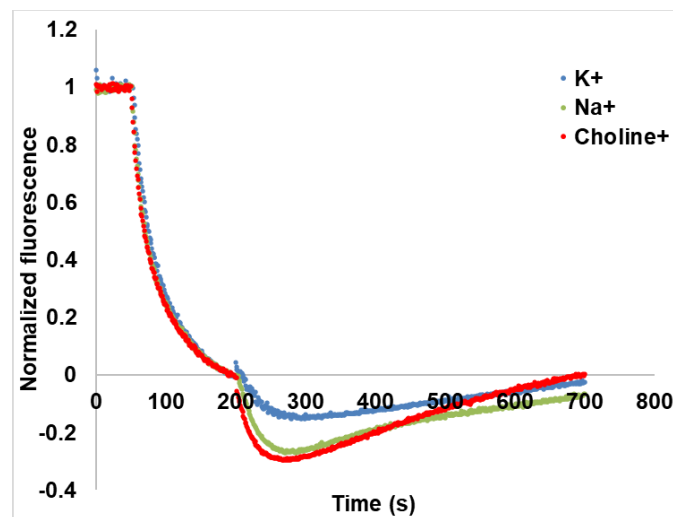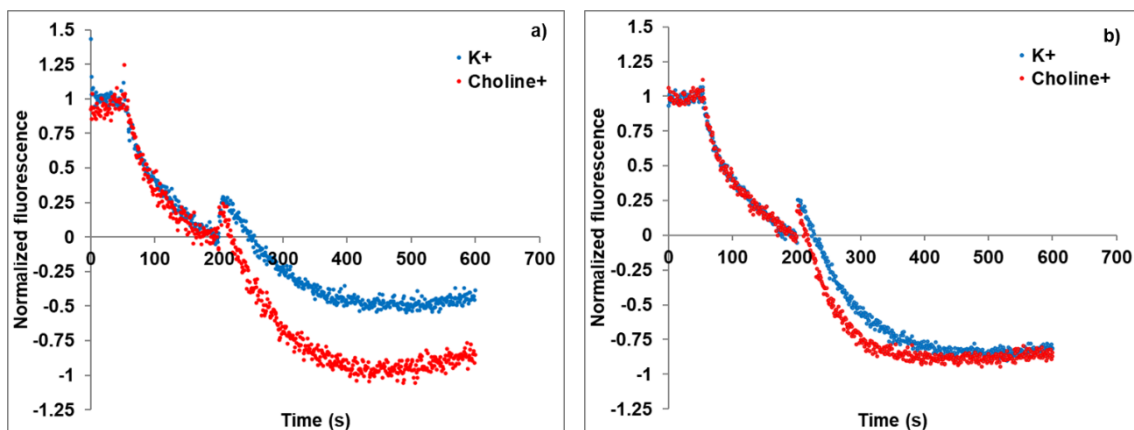

Figure 25: Comparison of normalized fluorescence flux curves for vesicles prepared from Knabc cell expressing YjbQ orthologous protein from *S. aureus* (K$^+$ and choline$^+$). Protein expression was done a) in the absence or b) presence of DAC domain.

We concluded that the selected orthologous proteins are not good candidates to study the properties of YjbQ. It is also possible that we needed to optimize the conditions that maximize protein expression of the orthologs.

4.1.8 Final considerations regarding the *in vitro* fluorescence-based flux assays

Overall, from these *in vitro* fluorescence-based flux assays, we concluded that YjbQ is selective for K$^+$. It is able to transport Na$^+$, even though with lower efficiency. YjbQ has increased activity at high pH values (8.5-9.0), and importantly, c-di-AMP binding inhibits YjbQ function. At pH 8.5, K$_{1/2}$ of c-di-AMP inactivation is ~2 µM, which is on the lower range of described concentrations for c-di-AMP in *B. subtilis* (1-10 µM).

4.2 *In vivo* growth experiments in *Bacillus subtillis*

To study the functional properties of YjbQ *in vivo*, growth experiments were performed in *Bacillus subtilis*, in a strain where the gene that encodes for the transporter was replaced by a kanamycin resistance cassette. This 168Δ*yjbQ* strain was created by transforming the laboratory strain 168 with a PCR fragment spanning the kanamycin resistance cassette together with ~600 bp of the *B. subtilis* genome that flank *yjbQ*. In addition, we cloned the *yjbQ* gene in the pBS0E plasmid, creating pBS0E-*yjbQ*, which allows bacitracin induced over-expression from a replicative plasmid. Both the empty plasmid (pBS0E) and the pBS0E-*yjbQ* construct were transformed into strain 168Δ*yjbQ*, creating strains 168Δ*yjbQ*+pBS0E and 168Δ*yjbQ*+pBS0E-*yjbQ*. Overall, we generated and tested 3 different clones for each strain.

We confirmed the *yjbQ* deletion by PCR using genomic DNA as template alongside wild-type *B. subtilis* genomic DNA and with primers designed to anneal about 600 base pairs upstream and downstream of *yjbQ*. The obtained amplified genetic product was evaluated by agarose electrophoresis (Figure 26). All mutant colonies showed a product that is smaller than the PCR from genomic DNA from the wild-type strain and has the expected molecular weight of the kanamycin cassette and flanking regions, around 2500 bp compared to 3000 bp from WT.
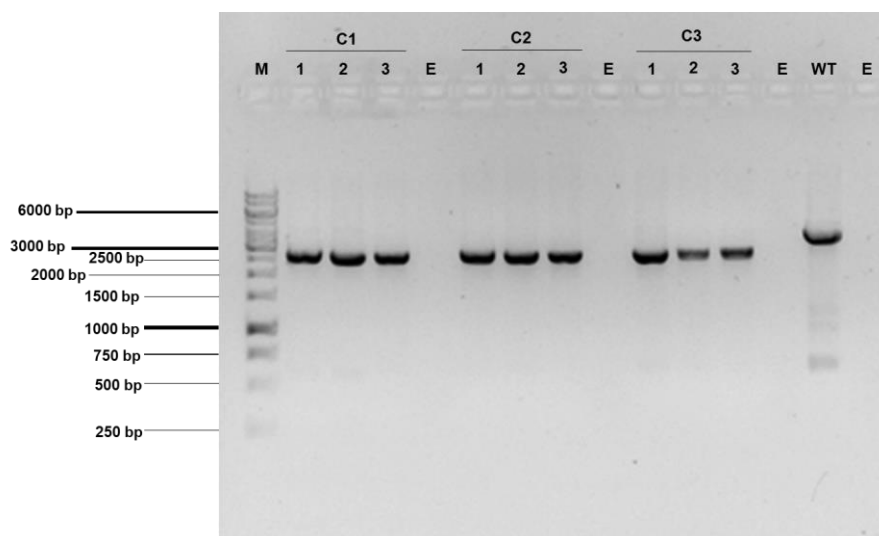
Figure 26: Agarose gel electrophoresis of PCR products from genomic DNA of deletion mutant clones (168Δ*yjbQ*). M: Marker (DNA ladder); E: Empty lane; WT: Wild Type; C1: Colony 1; C2: Colony 2; C3: Colony 3; Lanes marked as 1, 2 and 3 (either for C1, C2, C3 colonies) correspond to different amounts (1, 2 or 3 μL) of PCR template.

To understand how the presence of the transporter influences growth at different pH values and in different concentrations of potassium, we monitored growths in either minimal media or YPD media.

4.2.1 Growths at pH 7.0

These experiments were performed in 96-wells plates with SMM media at pH 7.0 with strains 168, 168Δ*yjbQ*, 168Δ*yjbQ*+pBS0E and 168Δ*yjbQ*+pBS0E-*yjbQ* and regular monitoring of $OD_{600\ nm}$. As it can be observed in Figure 27, there are no differences between growths with and without bacitracin and either high or low K^+ concentrations. The only hint of an effect appears to reside on a slightly longer lag phase when bacitracin is added to 168Δ*yjbQ*+pBS0E and 168Δ*yjbQ*+pBS0E-*yjbQ* strains relative to strains 168 and 168Δ*yjbQ*. Since bacitracin is the inducer of the pBS0E plasmid, this may cause some delay on cellular growth as expression is likely to channel resources away from growth, as previously discussed (Diaz Ricci & Hernández, 2000; Wang et al., 2006), impacting metabolism by favoring protein synthesis while sacrificing cellular growth (Aucoin et al., 2006). Another possible explanation for this difference is the presence of three antibiotics, kanamycin, lincomycin and erythromycin when the pBS0E plasmid is present, compared to only kanamycin in the case of 168Δ*yjbQ* strain and no antibiotic at

all in the case of 168 strain alone. This may increase the stress levels imposed on the growing cells (Diaz Ricci & Hernández, 2000).

Figure 27: Growth curves in SMM medium pH 7.0 for strains 168, 168Δ*yjbQ*, 168Δ*yjbQ*+pBS0E, 168Δ*yjbQ*+pBS0E-*yjbQ*. "Control" corresponds to medium without inoculated cells. A: 0.5 mM K^+ without bacitracin. B: 100 mM K^+ without bacitracin. C: 0.5 mM K^+ with bacitracin. D: 100 mM K^+ with bacitracin. Mean and standard deviation are shown for 3 technical replicas.

From the same experiment, we also compared the growth curves for 168Δ*yjbQ*+pBS0E-*yjbQ* 168Δ*yjbQ*+pBS0E with and without bacitracin in the two different K^+ concentrations (Figure 28). Once again there is no variation between conditions.
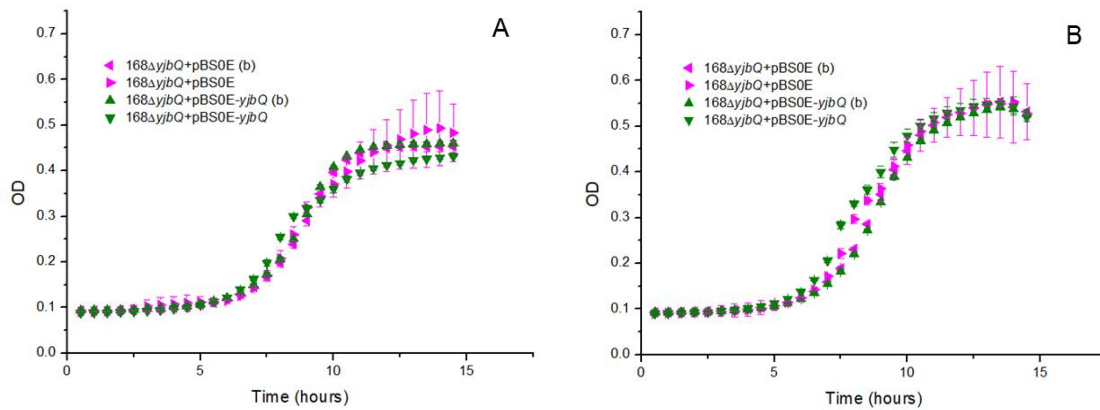
Figure 28: Growth curves at pH 7.0 in SMM medium for strains 168Δ*yjbQ*+pBS0E, 168Δ*yjbQ*+pBS0E-*yjbQ*. A: 0.5 mM K⁺, in the absence and presence of bacitracin (indicated as "(b)"). B: 100 mM K⁺, in the absence and presence of bacitracin (indicated as "(b)"). Mean and standard deviation are shown for 3 technical replicas.

4.2.2 Growths at pH 9.0

Growths at pH 9.0 (Figure 29) were performed in YPD with 100 mM Bis-tris propane buffer, with either 0.5 mM or 100 mM K⁺. All conditions contained bacitracin. Once again, there was practically no difference, between the background strain (168) and the deletion mutant (168Δ*yjbQ*), in both concentrations of K⁺. This means that at pH 9.0, the absence of the transporter does not disturb the growth of the cells.

In contrast, 168Δ*yjbQ*+pBS0E and168Δ*yjbQ*+pBS0E-*yjbQ*, appear to show a slight difference in the growth lag phase. Over-expression of the transporter reduced the lag phase relative to the strain with the empty plasmid, at either 0.5 mM or 100 mM K⁺ concentrations. In addition, higher K⁺ reduces the lag phase and this effect is potentiated by expression of the transporter.
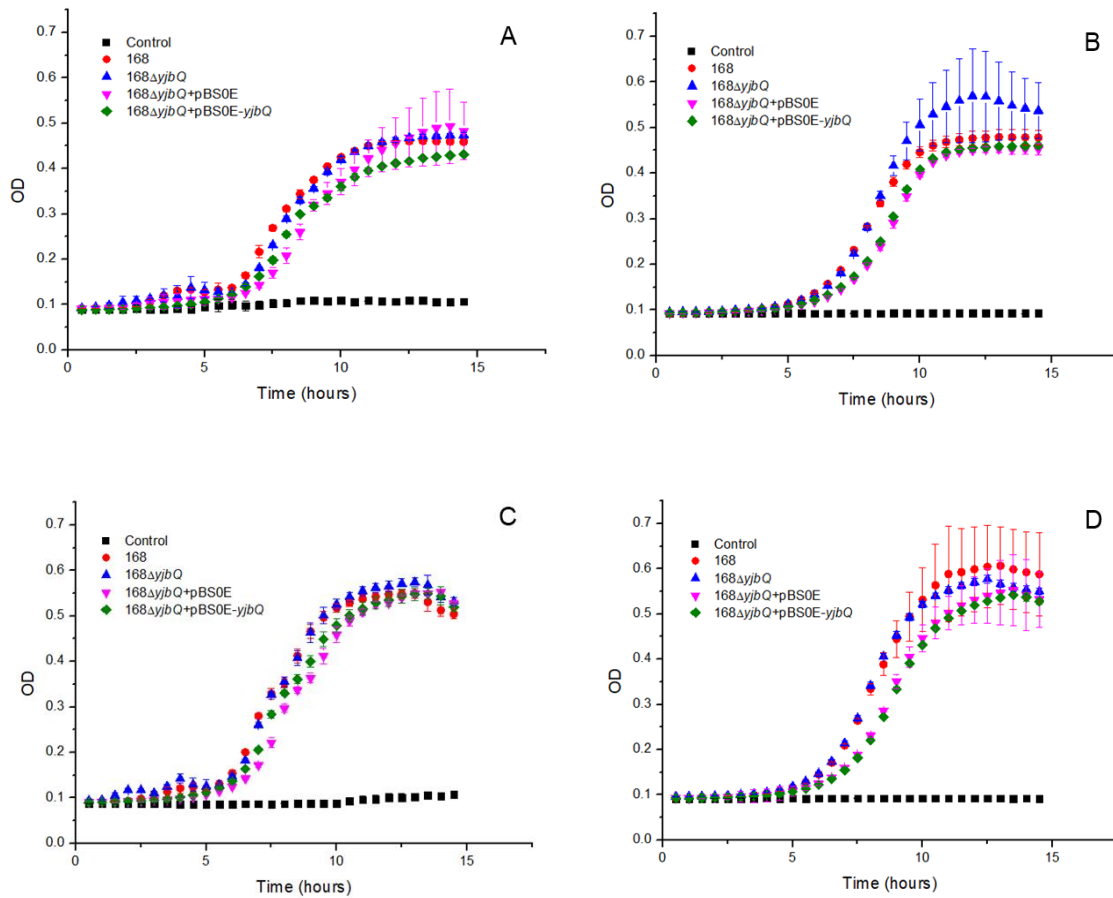
Figure 29: Growth curves in YPD medium pH 9.0 for strains 168, 168Δ*yjbQ*, 168Δ*yjbQ*+pBS0E, 168Δ*yjbQ*+pBS0E-*yjbQ*. "Control" corresponds to medium without inoculated cells. A: With 0.5 mM K$^+$. B: With 100 mM K$^+$. C: Comparison of 168Δ*yjbQ*+pBS0E and 168Δ*yjbQ*+pBS0E-*yjbQ* in both K$^+$ conditions (0.5 mM and 100 mM). Mean and standard deviation are shown for 3 technical replicas.

4.2.3 Growths at pH 5.5

Growths in YPD at pH 5.5 (100 mM MES buffer), are shown in Figure 30. A noticeable difference is observed between strains 168 and 168Δ*yjbQ* relative to strains transformed with pBS0E plasmid. Moreover, in this first experiment there was no growth in media with 0.5 mM K$^+$ when YjbQ is over-expressed, with the curve coinciding with the empty medium (Control). In addition, growth was also considerably affected in the strain with empty plasmid.
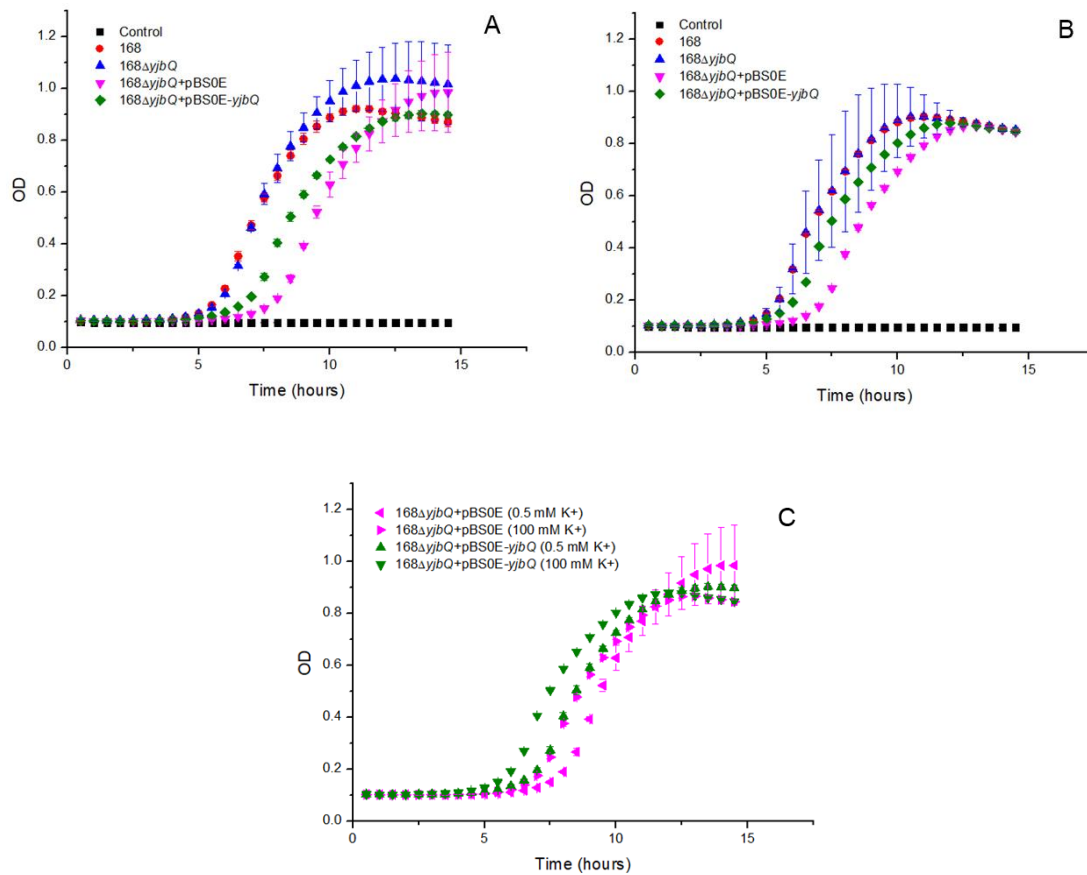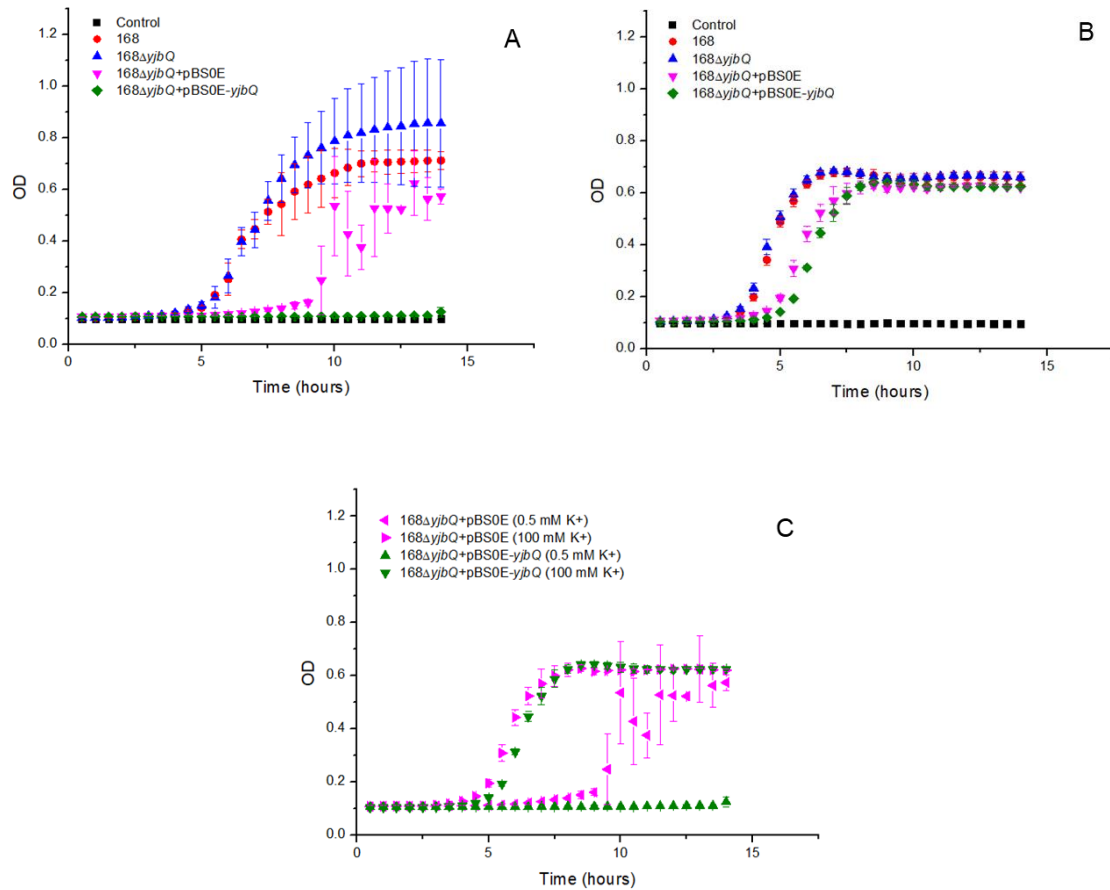
Figure 30: Growth curves in YPD medium pH 5.5 for strains 168, 168Δ*yjbQ*, 168Δ*yjbQ*+pBS0E, 168Δ*yjbQ*+pBS0E-*yjbQ*. "Control" corresponds to medium without inoculated cells. A: With 0.5 mM K$^+$. B: With 100 mM K$^+$. C: Comparison of 168Δ*yjbQ*+pBS0E and 168Δ*yjbQ*+pBS0E-*yjbQ* in both K$^+$ conditions (0.5 mM and 100 mM). Mean and standard deviation are shown for 3 technical replicas.

We hypothesized that the presence of the transporter could provoke this difference; therefore, YjbQ could be playing a significant role at low pH. This effect is uncommon for K$^+$/H$^+$ antiporters, which have been reported to be involved in alkaline stress, pumping protons into the cytosol in exchange for K$^+$ to maintain the intracellular environment closer to neutral pH (Plack & Rosen, 1980; Radchenko et al., 2006; Krulwich et al., 2011). However, if YjbQ is instead involved in the uptake of K$^+$ and extrusion of H$^+$, this would be coherent with the fact that K$^+$ uptake systems are key to adapt to acidic environmental conditions (Trchounian & Kobayashi, 1999).

In the following experiments we increased the lower K$^+$ concentration to a higher value, from 0.5 to 2 mM K$^+$, to check whether the effect was still observed.

Experiment performed at pH 5.5, with MES buffer, contrasting 2 mM and 100 mM K⁺ concentrations are presented in Figure 31. Besides strain 168 and the technical triplicates for all strains, this plate included biological duplicates for 168Δ*yjbQ* (colonies 1 and 2), 168Δ*yjbQ*+pBS0E (colonies 1 and 2) and 168Δ*yjbQ*+pBS0E-*yjbQ* (colonies 1 and 2). The effect observed in Figure 30 was no longer observed, as no growth curve decreased towards the Control level. In general, there was no worthy difference detected.

Figure 31: Growth curves in YPD medium pH 5.5 for strains 168, 168Δ*yjbQ*, 168Δ*yjbQ*+pBS0E, 168Δ*yjbQ*+pBS0E-*yjbQ*. A: With 2 mM K⁺. B: With 100 mM K⁺. "Control" corresponds to medium without inoculated cells. Biological duplicates were included for strains 168Δ*yjbQ*, 168Δ*yjbQ*+pBS0E and 168Δ*yjbQ*+pBS0E-*yjbQ*. Mean and standard deviation are shown for 3 technical replicas.

This was made clearer by isolating growth curves in Figure 32. Strain 168 and biological duplicates of 168Δ*yjbQ* coincided, at either 2 mM K⁺ or 100 mM K⁺. Comparison between YjbQ over-expression and strain with the empty plasmid showed that differences disappeared when considering that biological duplicates also showed similar variations.
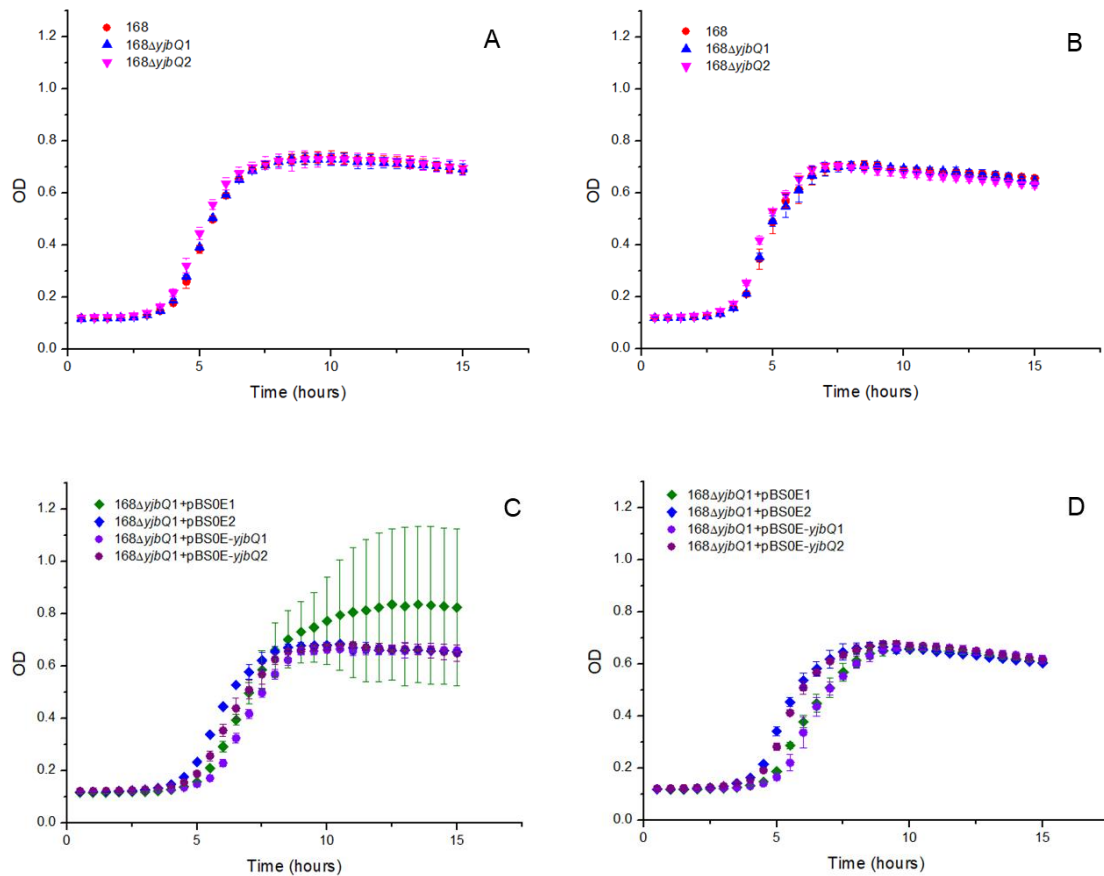
Figure 32 Growth curves in YPD medium pH 5.5 of biological duplicates from strains 168Δ*yjbQ*+pBS0E 168Δ*yjbQ*+pBS0E-*yjbQ*. A: Comparison of strains 168 and 168Δ*yjbQ*1 and 168Δ*yjbQ*2 in 2 mM K⁺. B Comparison of strains 168 and 168Δ*yjbQ*1 and 168Δ*yjbQ*2 in 100 mM K⁺. C: Comparison of strains 168Δ*yjbQ*+pBS0E1, 168Δ*yjbQ*+pBS0E2,168Δ*yjbQ*+pBS0E-*yjbQ*1 and 168Δ*yjbQ*+pBS0E-*yjbQ*2 in 2 mM K⁺. D: Comparison of strains 168Δ*yjbQ*+pBS0E1, 168Δ*yjbQ*+pBS0E2,168Δ*yjbQ*+pBS0E-*yjbQ*1 and 168Δ*yjbQ*+pBS0E-*yjbQ*2 in 100 mM K⁺. Biological duplicates were included for strains 168Δ*yjbQ*, 168Δ*yjbQ*+pBS0E and 168Δ*yjbQ*+pBS0E-*yjbQ*. Mean and standard deviation are shown for 3 technical replicas.

We repeated the pH 5.5 conditions with 0.5 mM K⁺ and 100 mM K⁺, as for the first experiment, but this time including biological triplicates. Strain 168 was not included due to space limitations in the plate and because in all previous experiments this strain overlapped with the deletion mutant strain. The results of this experiment are shown in Figure 33. It is immediately obvious that the lack of growth originally observed with 0.5 mM (Figure 30) was no longer observed, suggesting that it might have been the result of manipulation error.
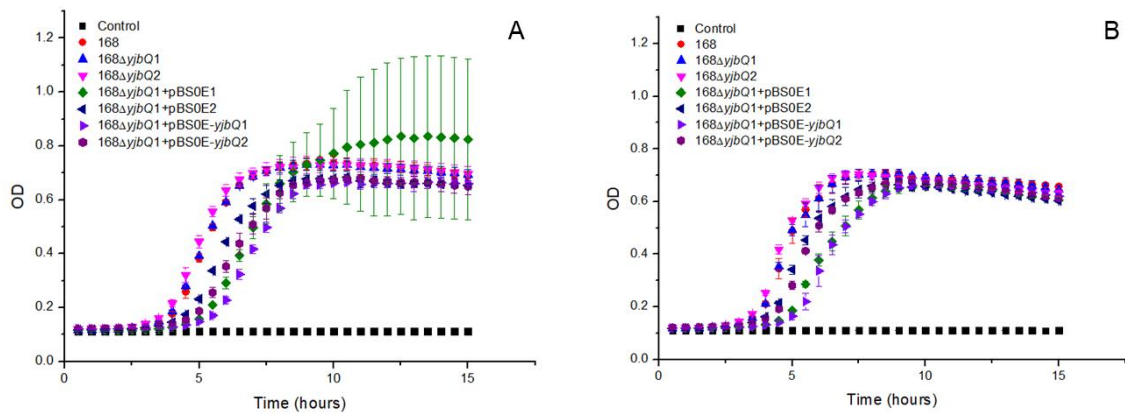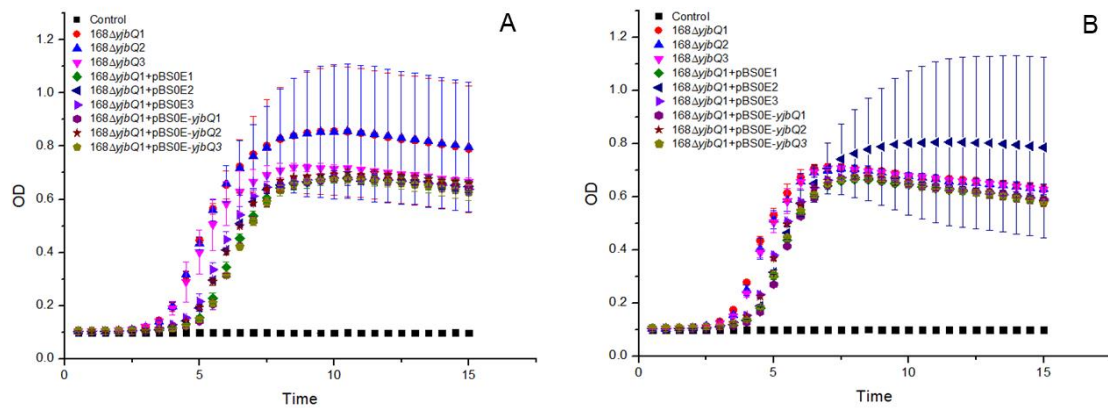
Figure 33: Growth curves in YPD medium pH 5.5 from strains 168Δ*yjbQ*, 168Δ*yjbQ*+pBS0E, 168Δ*yjbQ*+pBS0E-*yjbQ*. A: With 0.5 mM K$^+$. B: With 100 mM K$^+$. "Control" corresponds to medium without inoculated cells. Biological triplicates were included for strains 168Δ*yjbQ*, 168Δ*yjbQ*+pBS0E and 168Δ*yjbQ*+pBS0E-*yjbQ*. Mean and standard deviation are shown for 3 technical replicas.

We also performed comparisons to better observe the similarities or variations among the biological triplicates at both K$^+$ concentrations (Figure 34). In all cases, the biological triplicates behaved similarly with only some outlier measurements in the stationary phase.
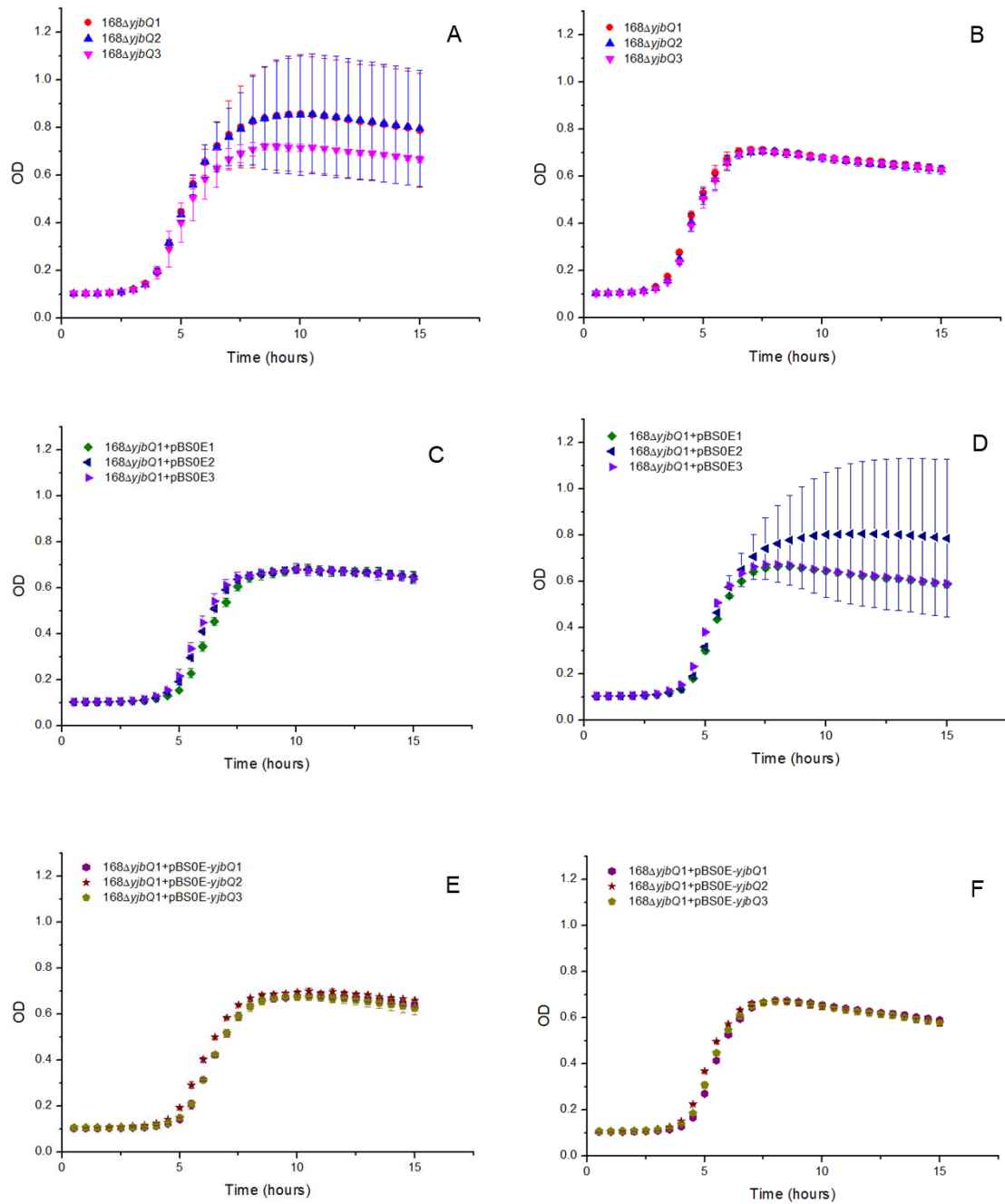
Figure 34: Growth curves in YPD medium pH 5.5 of biological triplicates from strains 168Δ*yjbQ*, 168Δ*yjbQ*+pBS0E, 168Δ*yjbQ*+pBS0E-*yjbQ*. A: Comparison of biological replicas for strain 168Δ*yjbQ* in 0.5 mM K$^+$. B: Comparison of biological replicas for strain 168Δ*yjbQ* in 100 mM K$^+$. C: Comparison of biological replicas for strain 168Δ*yjbQ*+pBS0E in 0.5 mM K$^+$. D: Comparison of biological replicas for strain 168Δ*yjbQ*+pBS0E in 100 mM K$^+$. E: Comparison of biological for strains 168Δ*yjbQ*+pBS0E-*yjbQ* in 0.5 mM K$^+$. F: Comparison of biological replicas for strains 168Δ*yjbQ*+pBS0E-*yjbQ* in 100 mM K$^+$. Mean and standard deviation are shown for 3 technical replicas.

Finally, we compared the biological triplicates of strain 168Δ*yjbQ*+pBS0E with strain 168Δ*yjbQ*+pBS0E-*yjbQ* at both concentrations of K$^+$ (0.5 mM and 100 mM) in Figure 35. Again, there are no growth changes caused by over-expression of YjbQ.
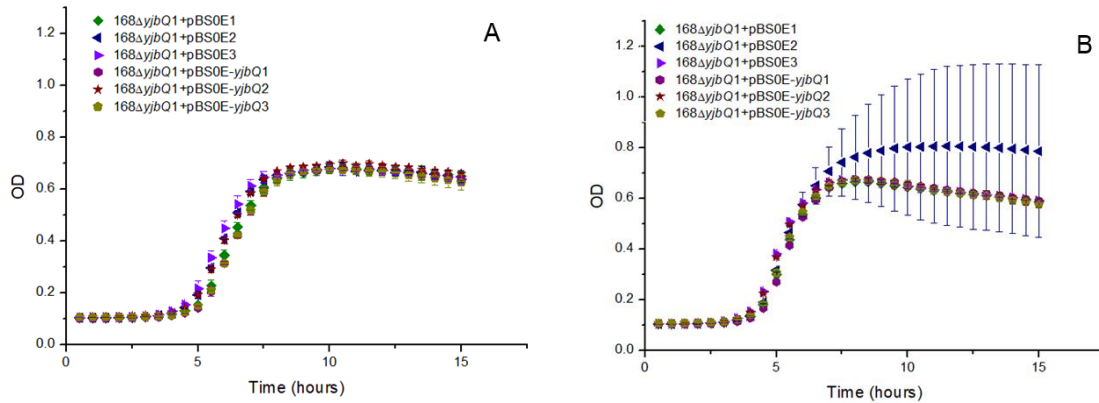
Figure 35: Growth curves in YPD medium pH 5.5 for strains 168Δ*yjbQ*+pBS0E and 168Δ*yjbQ*+pBS0E-*yjbQ*. A: Comparison of biological replicas for strains 168Δ*yjbQ*+pBS0E and 168Δ*yjbQ*+pBS0E-*yjbQ* in 0.5 mM K$^+$. B: Comparison of biological replicas for strains 168Δ*yjbQ*+pBS0E and 168Δ*yjbQ*+pBS0E-*yjbQ* in 100 mM K$^+$. Mean and standard deviation are shown for 3 technical replicas.

4.2.4 Final considerations regarding the growth experiments

With these experiments we were hoping to demonstrate a physiological role for YjbQ. We could only observe a small effect of YjbQ over-expression at pH 9.0. The lag phase was reduced in the presence of the transporter and importantly this effect is K$^+$ concentration dependent, reflecting observations with the other *B. subtilis* K$^+$/H$^+$ antiporter KhtTU (Cereija et al., 2021). These experiments should be repeated with biological replicas to ensure that the effect is not colony dependent. Importantly, we saw no phenotype for deletion of the transporter as if it is very poorly expressed in wild-type cells or is mostly inactive. One aspect that we could not control in these growth studies is the c-di-AMP concentration. Our *in vitro* results have shown c-di-AMP inhibits YjbQ and therefore, and it is possible that the lack of phenotype results from having a wild-type transporter that is mainly inactive. To test this, we should over-express the YjbQ-H585A mutant and analyze its impact on growth, as described here for the wild-type protein.

5.Conclusions

This work was done with the aim of better understanding the function of YjbQ, namely its ion selectivity, pH and c-di-AMP dependence. Additionally, we wanted to understand if the presence of YjbQ was advantageous for *Bacillus subtilis* under alkaline and/or acidic stress. In parallel, we were curious to verify whether the same observed functional properties were present on orthologous proteins from closely related species (*Mesobacillus foraminis*, *Metabacillus litoralis*, *Staphylococcus aureus*). Experiments *in vitro* and *in vivo* were set, involving fluorescence-flux based assays and monitoring growth in *Bacillus subtilis* strains, respectively.

From the results obtained *in vitro*, it is possible to conclude that the activity of YjbQ is affected by variations in pH, increasing at higher pH. It was also noted that YjbQ transports preferentially potassium ions, although sodium ions are also allowed. The addition of c-di-AMP had an inhibitory effect on K^+ transport, an indication that was sustained from analysing the function of a YjbQ mutant with a disrupted c-di-AMP binding site.

In terms of future perspectives, it is desirable to use a different approach for the *in vitro* characterization since the signal we get from everted vesicles with YjbQ is relatively small and is "contaminated" by signal from other proteins in the membrane of the vesicle. An alternative that is worthwhile exploring is to express and purify YjbQ in detergent and reconstitute the protein in proteoliposomes. Using fluorescence-based flux assays already established in the laboratory it would be possible to confirm the c-di-AMP effect, define if K^+/H^+ antiport is electroneutral or electrogenic and define more precisely the regulation by pH. In addition, it is important to confirm the impact of the H585A mutation on the binding of c-di-AMP by expressing the RCK domain (already done in the laboratory) and determining the ligand affinity by isothermal calorimetry. The effect of other mutants in the binding pocket could be characterized in this way and then explored in the function of the full-length protein. Finally, to understand the physiological role of YjbQ we propose to use mutants in the c-di-AMP binding pocket to avoid regulation by c-di-AMP, ensuring that the protein is fully active during the analysis.

References

Albertini, A. M., & Galizzi, A. (1999). The sequence of the *trp* operon of *Bacillus subtilis* 168 (*trpC2*) revisited. *Microbiology (Reading, England)*, *145 (Pt 12)*, 3319–3320. https://doi.org/10.1099/00221287-145-12-3319

Albright, R. A., Ibar, J. L., Kim, C. U., Gruner, S. M., & Morais-Cabral, J. H. (2006). The RCK domain of the KtrAB K+ transporter: multiple conformations of an octameric ring. *Cell*, *126*(6), 1147–1159. https://doi.org/10.1016/j.cell.2006.08.028

Ashcroft, F., Gadsby, D., & Miller, C. (2009). Introduction. The blurred boundary between channels and transporters. *Philosophical transactions of the Royal Society of London. Series B, Biological sciences*, *364*(1514), 145–147. https://doi.org/10.1098/rstb.2008.0245

Aucoin, M. G., McMurray-Beaulieu, V., Poulin, F., Boivin, E. B., Chen, J., Ardelean, F. M., Cloutier, M., Choi, Y. J., Miguez, C. B., & Jolicoeur, M. (2006). Identifying conditions for inducible protein production in E. coli: combining a fed-batch and multiple induction approach. *Microbial cell factories*, *5*, 27. https://doi.org/10.1186/1475-2859-5-27

Bai, Y., Yang, J., Zarrella, T. M., Zhang, Y., Metzger, D. W., & Bai, G. (2014). Cyclic di-AMP impairs potassium uptake mediated by a cyclic di-AMP binding protein in Streptococcus pneumoniae. *Journal of bacteriology*, *196*(3), 614–623. https://doi.org/10.1128/JB.01041-13

Bakker, E. P., & Mangerich, W. E. (1981). Interconversion of components of the bacterial proton motive force by electrogenic potassium transport. *Journal of bacteriology*, *147*(3), 820–826. https://doi.org/10.1128/jb.147.3.820-826.1981

Beagle, S. D., & Lockless, S. W. (2021). Unappreciated Roles for K+ Channels in Bacterial Physiology. *Trends in microbiology*, *29*(10), 942–950. https://doi.org/10.1016/j.tim.2020.11.005

Biocompare: The Buyer's Guide for Life Scientists. (n.d.). Retrieved September 16, 2022, from https://www.biocompare.com/11118-Chemically-Competent-Cells-10sup9sup-Efficiency/346522-NEB-5alpha-Competent-Ecoli-High-Efficiency/

Boudker, O., & Verdon, G. (2010). Structural perspectives on secondary active transporters. *Trends in pharmacological sciences*, *31*(9), 418–426. https://doi.org/10.1016/j.tips.2010.06.004

Cereija, T. B., Guerra, J., Jorge, J., & Morais-Cabral, J. H. (2021). c-di-AMP, a likely master regulator of bacterial K$^+$ homeostasis machinery, activates a K$^+$ exporter. *Proceedings of the National Academy of Sciences of the United States of America*, *118*(14), e2020653118. https://doi.org/10.1073/pnas.2020653118

Chin, K. H., Liang, J. M., Yang, J. G., Shih, M. S., Tu, Z. L., Wang, Y. C., Sun, X. H., Hu, N. J., Liang, Z. X., Dow, J. M., Ryan, R. P., & Chou, S. H. (2015). Structural Insights into the Distinct Binding Mode of Cyclic Di-AMP with SaCpaA_RCK. *Biochemistry*, *54*(31), 4936–4951. https://doi.org/10.1021/acs.biochem.5b00633

Corrigan, R. M., & Gründling, A. (2013). Cyclic di-AMP: another second messenger enters the fray. *Nature reviews. Microbiology*, *11*(8), 513–524. https://doi.org/10.1038/nrmicro3069

cpaA. (n.d.). Retrieved September 12, 2022, from http://subtiwiki.uni-goettingen.de/v4/gene?id=6985ED02AC7A04D4FD5E531C47DD4D1711D7F829

Cuello, L. G., Jogini, V., Cortes, D. M., & Perozo, E. (2010). Structural mechanism of C-type inactivation in K(+) channels. *Nature*, *466*(7303), 203–208. https://doi.org/10.1038/nature09153

Cuello, L. G., Romero, J. G., Cortes, D. M., & Perozo, E. (1998). pH-dependent gating in the Streptomyces lividans K+ channel. *Biochemistry*, *37*(10), 3229–3236. https://doi.org/10.1021/bi972997x

Diaz Ricci, J. C., & Hernández, M. E. (2000). Plasmid effects on Escherichia coli metabolism. *Critical reviews in biotechnology*, *20*(2), 79–108. https://doi.org/10.1080/07388550008984167

Diskowski, M., Mehdipour, A. R., Wunnicke, D., Mills, D. J., Mikusevic, V., Bärland, N., Hoffmann, J., Morgner, N., Steinhoff, H. J., Hummer, G., Vonck, J., & Hänelt, I. (2017). Helical jackknives control the gates of the double-pore K$^+$ uptake system KtrAB. *eLife*, *6*, e24303. https://doi.org/10.7554/eLife.24303

Doyle, D. A., Morais Cabral, J., Pfuetzner, R. A., Kuo, A., Gulbis, J. M., Cohen, S. L., Chait, B. T., & MacKinnon, R. (1998). The structure of the potassium channel: molecular basis of K+ conduction and selectivity. *Science (New York, N.Y.)*, *280*(5360), 69–77. https://doi.org/10.1126/science.280.5360.69

Earl, A. M., Losick, R., & Kolter, R. (2008). Ecology and genomics of Bacillus subtilis. *Trends in microbiology*, *16*(6), 269–275. https://doi.org/10.1016/j.tim.2008.03.004

Epstein W. (2003). The roles and regulation of potassium in bacteria. *Progress in nucleic acid research and molecular biology*, *75*, 293–320. https://doi.org/10.1016/s0079-6603(03)75008-9

Fahmi, T., Port, G. C., & Cho, K. H. (2017). c-di-AMP: An Essential Molecule in the Signaling Pathways that Regulate the Viability and Virulence of Gram-Positive Bacteria. *Genes*, *8*(8), 197. https://doi.org/10.3390/genes8080197

Forrest, L. R., Krämer, R., & Ziegler, C. (2011). The structural basis of secondary active transport mechanisms. *Biochimica et biophysica acta*, *1807*(2), 167–188. https://doi.org/10.1016/j.bbabio.2010.10.014

Fujisawa, M., Ito, M., & Krulwich, T. A. (2007). Three two-component transporters with channel-like properties have monovalent cation/proton antiport activity. *Proceedings of the National Academy of Sciences of the United States of America*, *104*(33), 13289–13294. https://doi.org/10.1073/pnas.0703709104

Gibhardt, J., Heidemann, J. L., Bremenkamp, R., Rosenberg, J., Seifert, R., Kaever, V., Ficner, R., & Commichau, F. M. (2020). An extracytoplasmic protein and a moonlighting enzyme modulate synthesis of c-di-AMP in Listeria monocytogenes. *Environmental microbiology*, *22*(7), 2771–2791. https://doi.org/10.1111/1462-2920.15008

Gibhardt, J., Hoffmann, G., Turdiev, A., Wang, M., Lee, V. T., & Commichau, F. M. (2019). c-di-AMP assists osmoadaptation by regulating the *Listeria monocytogenes* potassium transporters KimA and KtrCD. *The Journal of biological chemistry*, *294*(44), 16020–16033. https://doi.org/10.1074/jbc.RA119.010046

Giraldez, T., & Rothberg, B. S. (2017). Understanding the conformational motions of RCK gating rings. *The Journal of general physiology*, *149*(4), 431–441. https://doi.org/10.1085/jgp.201611726

Goldin A. L. (2003). Mechanisms of sodium channel inactivation. *Current opinion in neurobiology*, *13*(3), 284–290. https://doi.org/10.1016/s0959-4388(03)00065-5

Gu, H. J., Sun, Q. L., Luo, J. C., Zhang, J., & Sun, L. (2019). A First Study of the Virulence Potential of a *Bacillus subtilis* Isolate From Deep-Sea Hydrothermal Vent. *Frontiers in cellular and infection microbiology*, *9*, 183. https://doi.org/10.3389/fcimb.2019.00183

Gundlach, J., Herzberg, C., Kaever, V., Gunka, K., Hoffmann, T., Weiß, M., Gibhardt, J., Thürmer, A., Hertel, D., Daniel, R., Bremer, E., Commichau, F. M., & Stülke, J. (2017). Control of potassium homeostasis is an essential function of the second messenger cyclic di-AMP in *Bacillus subtilis*. *Science signaling*, *10*(475), eaal3011. https://doi.org/10.1126/scisignal.aal3011

Gundlach, J., Krüger, L., Herzberg, C., Turdiev, A., Poehlein, A., Tascón, I., Weiss, M., Hertel, D., Daniel, R., Hänelt, I., Lee, V. T., & Stülke, J. (2019). Sustained sensing in potassium homeostasis: Cyclic di-AMP controls potassium uptake by KimA at the levels of expression and activity. *The Journal of biological chemistry*, *294*(24), 9605–9614. https://doi.org/10.1074/jbc.RA119.008774

Hille B. (1972). The permeability of the sodium channel to metal cations in myelinated nerve. *The Journal of general physiology*, *59*(6), 637–658. https://doi.org/10.1085/jgp.59.6.637

Hoffmann, T., & Bremer, E. (2016, August 12). Management of Osmotic Stress by *Bacillus Subtilis*: Genetics and Physiology. *Stress and Environmental Regulation of Genekuang Expression and Adaptation in Bacteria*, 657–676. https://doi.org/10.1002/9781119004813.ch63

Holtmann, G., Bakker, E. P., Uozumi, N., & Bremer, E. (2003). KtrAB and KtrCD: two K+ uptake systems in Bacillus subtilis and their role in adaptation to hypertonicity. *Journal of bacteriology*, *185*(4), 1289–1298. https://doi.org/10.1128/JB.185.4.1289-1298.2003

Kalia, D., Merey, G., Nakayama, S., Zheng, Y., Zhou, J., Luo, Y., Guo, M., Roembke, B. T., & Sintim, H. O. (2013). Nucleotide, c-di-GMP, c-di-AMP, cGMP, cAMP, (p)ppGpp signaling in bacteria and implications in pathogenesis. *Chemical Society reviews*, *42*(1), 305–341. https://doi.org/10.1039/c2cs35206k

Kovács Á. T. (2019). Bacillus subtilis. *Trends in microbiology*, *27*(8), 724–725. https://doi.org/10.1016/j.tim.2019.03.008

Krulwich, T. A., Sachs, G., & Padan, E. (2011). Molecular aspects of bacterial pH sensing and homeostasis. *Nature reviews. Microbiology*, *9*(5), 330–343. https://doi.org/10.1038/nrmicro2549

Kuang, Q., Purhonen, P., & Hebert, H. (2015). Structure of potassium channels. *Cellular and molecular life sciences : CMLS*, *72*(19), 3677–3693. https://doi.org/10.1007/s00018-015-1948-5

MacKinnon R. (2003). Potassium channels. *FEBS letters*, *555*(1), 62–65. https://doi.org/10.1016/s0014-5793(03)01104-9

Masrati, G., Dwivedi, M., Rimon, A., Gluck-Margolin, Y., Kessel, A., Ashkenazy, H., Mayrose, I., Padan, E., & Ben-Tal, N. (2018). Broad phylogenetic analysis of cation/proton antiporters reveals transport determinants. *Nature communications*, *9*(1), 4205. https://doi.org/10.1038/s41467-018-06770-5

McRee, D. E. (1999, September 1). *Practical Protein Crystallography* (Second Edition). Elsevier Gezondheidszorg. https://doi.org/10.1016/B978-012486052-0/50005-1

Nakano, M. M., & Zuber, P. (1998). ANAEROBIC GROWTH OF A "STRICT AEROBE" (*BACILLUS SUBTILIS*). *Annual Review of Microbiology*, *52*(1), 165–190. https://doi.org/10.1146/annurev.micro.52.1.165

Nelson, J. W., Sudarsan, N., Furukawa, K., Weinberg, Z., Wang, J. X., & Breaker, R. R. (2013). Riboswitches in eubacteria sense the second messenger c-di-AMP. *Nature chemical biology*, *9*(12), 834–839. https://doi.org/10.1038/nchembio.1363

Newton, A. C., Bootman, M. D., & Scott, J. D. (2016). Second Messengers. *Cold Spring Harbor perspectives in biology*, *8*(8), a005926. https://doi.org/10.1101/cshperspect.a005926

Nozaki, K., Inaba, K., Kuroda, T., Tsuda, M., & Tsuchiya, T. (1996). Cloning and sequencing of the gene for Na+/H+ antiporter of Vibrio parahaemolyticus. *Biochemical and biophysical research communications*, *222*(3), 774–779. https://doi.org/10.1006/bbrc.1996.0820

Plack, R. H., Jr, & Rosen, B. P. (1980). Cation/proton antiport systems in Escherichia coli. Absence of potassium/proton antiporter activity in a pH-sensitive mutant. *The Journal of biological chemistry*, *255*(9), 3824–3825.

Prindle, A., Liu, J., Asally, M., Ly, S., Garcia-Ojalvo, J., & Süel, G. M. (2015). Ion channels enable electrical communication in bacterial communities. *Nature*, *527*(7576), 59–63. https://doi.org/10.1038/nature15709

Radchenko, M. V., Tanaka, K., Waditee, R., Oshimi, S., Matsuzaki, Y., Fukuhara, M., Kobayashi, H., Takabe, T., & Nakamura, T. (2006). Potassium/proton antiport system of Escherichia coli. *The Journal of biological chemistry*, *281*(29), 19822–19829. https://doi.org/10.1074/jbc.M600333200

Roosild, T. P., Castronovo, S., Miller, S., Li, C., Rasmussen, T., Bartlett, W., Gunasekera, B., Choe, S., & Booth, I. R. (2009). KTN (RCK) domains regulate K+ channels and transporters by controlling the dimer-hinge conformation. *Structure (London, England : 1993)*, *17*(6), 893–903. https://doi.org/10.1016/j.str.2009.03.018

Shao, L., Abdel-Motaal, H., Chen, J., Chen, H., Xu, T., Meng, L., Zhang, Z., Meng, F., & Jiang, J. (2018). Characterization of a Functionally Unknown Arginine-Aspartate-Aspartate Family Protein From *Halobacillus andaensis* and Functional Analysis of Its Conserved Arginine/Aspartate Residues. *Frontiers in microbiology*, *9*, 807. https://doi.org/10.3389/fmicb.2018.00807

Schoch, C. L., Ciufo, S., Domrachev, M., Hotton, C. L., Kannan, S., Khovanskaya, R., Leipe, D., Mcveigh, R., O'Neill, K., Robbertse, B., Sharma, S., Soussov, V., Sullivan, J. P., Sun, L., Turner, S., & Karsch-Mizrachi, I. (2020). NCBI Taxonomy: a comprehensive update on curation, resources and tools. *Database : the journal of biological databases and curation*, *2020*, baaa062. https://doi.org/10.1093/database/baaa062

Shrivastava, I. H., Tieleman, D. P., Biggin, P. C., & Sansom, M. S. (2002). K(+) versus Na(+) ions in a K channel selectivity filter: a simulation study. *Biophysical journal*, *83*(2), 633–645. https://doi.org/10.1016/s0006-3495(02)75197-7

Stautz, J., Hellmich, Y., Fuss, M. F., Silberberg, J. M., Devlin, J. R., Stockbridge, R. B., & Hänelt, I. (2021). Molecular Mechanisms for Bacterial Potassium Homeostasis. *Journal of molecular biology*, *433*(16), 166968. https://doi.org/10.1016/j.jmb.2021.166968

Stock, C., Hielkema, L., Tascón, I., Wunnicke, D., Oostergetel, G. T., Azkargorta, M., Paulino, C., & Hänelt, I. (2018). Cryo-EM structures of KdpFABC suggest a K+ transport mechanism via two inter-subunit half-channels. *Nature communications*, *9*(1), 4971. https://doi.org/10.1038/s41467-018-07319-2

Stülke, J., & Krüger, L. (2020). Cyclic di-AMP Signaling in Bacteria. *Annual review of microbiology*, *74*, 159–179. https://doi.org/10.1146/annurev-micro-020518-115943

Su, Y., Liu, C., Fang, H., & Zhang, D. (2020). Bacillus subtilis: a universal cell factory for industry, agriculture, biomaterials and medicine. *Microbial cell factories*, *19*(1), 173. https://doi.org/10.1186/s12934-020-01436-8

Tascón, I., Sousa, J. S., Corey, R. A., Mills, D. J., Griwatz, D., Aumüller, N., Mikusevic, V., Stansfeld, P. J., Vonck, J., & Hänelt, I. (2020). Structural basis of proton-coupled potassium transport in the KUP family. *Nature communications*, *11*(1), 626. https://doi.org/10.1038/s41467-020-14441-7

Teixeira-Duarte, C. M., Fonseca, F., & Morais-Cabral, J. H. (2019). Activation of a nucleotide-dependent RCK domain requires binding of a cation cofactor to a conserved site. *eLife*, *8*, e50661. https://doi.org/10.7554/eLife.50661

Trchounian, A., & Kobayashi, H. (1999). Kup is the major K+ uptake system in Escherichia coli upon hyper-osmotic stress at a low pH. *FEBS letters*, *447*(2-3), 144–148. https://doi.org/10.1016/s0014-5793(99)00288-4

Vieira-Pires, R. S., Szollosi, A., & Morais-Cabral, J. H. (2013). The structure of the KtrAB potassium transporter. *Nature*, 496(7445), 323–328. https://doi.org/10.1038/nature12055

Wang, Z., Xiang, L., Shao, J., Wegrzyn, A., & Wegrzyn, G. (2006). Effects of the presence of ColE1 plasmid DNA in Escherichia coli on the host cell metabolism. *Microbial cell factories*, *5*, 34. https://doi.org/10.1186/1475-2859-5-34

Whatmore, A. M., Chudek, J. A., & Reed, R. H. (1990). The effects of osmotic upshock on the intracellular solute pools of Bacillus subtilis. *Journal of general microbiology*, 136(12), 2527–2535. https://doi.org/10.1099/00221287-136-12-2527

Zaprasis, A., Brill, J., Thüring, M., Wünsche, G., Heun, M., Barzantny, H., Hoffmann, T., & Bremer, E. (2013). Osmoprotection of Bacillus subtilis through import and proteolysis of proline-containing peptides. *Applied and environmental microbiology*, *79*(2), 576–587. https://doi.org/10.1128/AEM.01934-12

Zarrella, T. M., & Bai, G. (2020). The Many Roles of the Bacterial Second Messenger Cyclic di-AMP in Adapting to Stress Cues. *Journal of bacteriology*, *203*(1), e00348-20. https://doi.org/10.1128/JB.00348-20

Zeigler, D. R., Prágai, Z., Rodriguez, S., Chevreux, B., Muffler, A., Albert, T., Bai, R., Wyss, M., & Perkins, J. B. (2008). The origins of 168, W23, and other Bacillus subtilis legacy strains. *Journal of bacteriology*, *190*(21), 6983–6995. https://doi.org/10.1128/JB.00722-08

Zhang, H., Pan, Y., Hu, L., Hudson, M. A., Hofstetter, K. S., Xu, Z., Rong, M., Wang, Z., Prasad, B., Lockless, S. W., Chiu, W., & Zhou, M. (2020). TrkA undergoes a tetramer-to-dimer conversion to open TrkH which enables changes in membrane potential. *Nature communications*, *11*(1), 547. https://doi.org/10.1038/s41467-019-14240-9